

$B_s \rightarrow K^{(*)} \ell \bar{\nu}$, Angular Analysis, S-wave Ccontributions and $|V_{ub}|$

Ulf-G. Meißner^{a,b} and Wei Wang^a

^a*Helmholtz-Institut für Strahlen- und Kernphysik and Bethe Center for Theoretical Physics, Universität Bonn, D-53115 Bonn, Germany*

^b*Institute for Advanced Simulation, Institut für Kernphysik and Jülich Center for Hadron Physics, JARA-FAME and JARA-HPC, Forschungszentrum Jülich, D-52425 Jülich, Germany*

E-mail: meissner@hiskp.uni-bonn.de, weiwang@hiskp.uni-bonn.de

ABSTRACT: We analyse the $\bar{B}_s^0 \rightarrow K^+ l^- \bar{\nu}$ and $\bar{B}_s^0 \rightarrow K^{*+} (\rightarrow K\pi) \ell^- \bar{\nu}$ decays that are valuable for extracting the CKM matrix element $|V_{ub}|$. We calculate the differential and integrated partial widths in units of $|V_{ub}|^2$ based on various calculations of hadronic form factors and in particular the latest Lattice QCD calculation of the $B_s \rightarrow K^*$ form factors. For the decay $\bar{B}_s^0 \rightarrow K\pi \ell \bar{\nu}$, we formulate the general angular distributions with the inclusion of the various partial-wave $K\pi$ contributions. Using the results for the $K\pi$ scalar form factor calculated from unitarized chiral perturbation theory, we explore the S-wave effects on angular distribution variables and demonstrate that they may not be negligible, considering the high precision expected in future measurements. We also briefly discuss the impact of the S-wave $\pi\pi$ contributions in the $B^- \rightarrow \pi^+ \pi^- \ell \bar{\nu}$ decay and provide estimates for the mode $B^- \rightarrow K^+ K^- \ell \bar{\nu}$. The studies of these channels in future can not only be used to determine $|V_{ub}|$, but may also provide valuable information on the $K\pi$ and $\pi\pi$ phase shifts.

Contents

1	Introduction	1
2	Form factors	3
3	$B_s \rightarrow K \ell \bar{\nu}_\ell$	7
4	Full angular distribution of $B_s \rightarrow K \pi \ell \bar{\nu}$	9
4.1	Differential and integrated decay widths	13
4.2	Distribution in θ_K	16
4.3	Distribution in θ_l and forward-backward asymmetry	17
4.4	Distribution in the azimuthal angle ϕ	18
4.5	Polarisation of the τ lepton	20
4.6	$B^- \rightarrow \pi^+ \pi^- \ell \bar{\nu}$	21
4.7	$B^- \rightarrow K^+ K^- \ell \bar{\nu}$	24
5	Conclusions	25
A	Angular coefficients	27

1 Introduction

The precision determination of the Cabibbo-Kobayashi-Maskawa (CKM) matrix element $|V_{ub}|$ is of particular importance to test the Standard Model description of CP violating effects. Such effects in weak decays are caused by the presence of an irreducible complex phase in the unitary 3×3 CKM matrix. $|V_{ub}|$ can be determined from a multitude of weak B -decays governed by the $b \rightarrow u$ transition which involve either inclusive or exclusive final states and exhibit different experimental or theoretical challenges. At the current stage, there is a tension between the values extracted from inclusive and exclusive decays. The inclusive determinations mostly yield a central value larger than 4×10^{-3} , while exclusive analyses produce central values below this (for a review, See Ref. [1, 2]). Though this tension is only about 3σ , it has already created a significant amount of speculations about possible new physics effects.

Currently, the process $B \rightarrow \pi l \nu_\ell$, with $l = e, \mu$, is considered the most reliable exclusive channel to extract $|V_{ub}|$ (for a recent update using light-cone sum rules (LCSR) see Ref. [3]). There is a steady progress in measuring the branching fraction and q^2 -distribution on the experimental side [4], while the theoretical precision is approaching two-loop accuracy in the QCD sum rules [5]. On the other hand, new channels that are able to extract $|V_{ub}|$ and thus can reduce statistical and systematic uncertainties also deserve theoretical and

experimental investigations. The $\overline{B}_s^0 \rightarrow K^+ \ell^- \bar{\nu}$ and $\overline{B}_s^0 \rightarrow K^{*+} \ell^- \bar{\nu}$ decays are of this type. In this work, we shall provide predictions of the differential and integrated decay widths in units of $|V_{ub}|^2$ using the state-of-the-art knowledge of the form factors; those include not only the recent Lattice QCD (LQCD) calculation [6] and the LCSR [7], but also various sets of results calculated from the factorisation approach [8] and QCD-inspired models [9–12].

Compared to the $B \rightarrow \pi \ell \bar{\nu}$ and $B_s \rightarrow K \ell \bar{\nu}$ decays, the $B \rightarrow \rho \ell \bar{\nu}$ and $B_s \rightarrow K^* \ell \bar{\nu}$ reactions receive an additional complexity due to the large width of ρ (about 150 MeV) and K^* (about 50 MeV) compared to the hadronic scale. These processes are quasi-four-body decays, and in principle other $K\pi/\pi\pi$ resonant and nonresonant states may also contribute in the same final state, and thus dilute the theoretical predictions. Another motivation of this work is to develop a general formalism to incorporate various partial-wave contributions (similar with the $B \rightarrow K_J^*(\rightarrow K\pi)\ell^+\ell^-$ case [13–22], see also Ref. [23–28]), through which the branching ratios, forward-backward asymmetries and polarisations can be projected out. In particular, it is worthwhile to stress that the S-wave, whose effects are not negligible as we will show in the following, can *not* be expressed in terms of a Breit-Wigner formula, especially for the broad scalar meson $\kappa \equiv K_0^*(800)$. The broad nature is also stressed from the Roy-Steiner representations of the πK scattering [29, 30]. To avoid such problem, we will make use of the Watson theorem which allows reliable description in terms of the scalar form factors. These scalar form factors have been calculated in dispersion theory or in unitarization methods applied to chiral perturbation theory [31–44].

Moreover, existing measurements of the branching ratio for the charged current mediated $B \rightarrow \tau \bar{\nu}_\tau$ process yield results which are systematically higher than the SM expectations [45–47]. The measured decay rate for $B \rightarrow D^{(*)} \tau \bar{\nu}$ is also above the SM value [48, 49]. B decays with τ leptons in the final state offer possibilities of significant new physics (NP) contributions not present in processes with light leptons, as the large τ mass can overcome the helicity suppression of certain decay amplitudes. In this respect, the $B_s \rightarrow K^* \tau \bar{\nu}_\tau$ and $B \rightarrow \rho \tau \bar{\nu}_\tau$ decays having two detectible particles of non-zero spin in the final state ($K^*/\rho, \tau$) offer the opportunity of an even more complete investigation of the structure of possible NP contributions. A number of experimental observables sensitive to possible NP effects can be introduced. In the present study, we explore several such observables, like the differential distribution over the lepton invariant mass, the longitudinal K^* branching fraction, the $K^* - \tau$ opening angle distribution, as well as the τ helicity fractions.

This paper is organised as follows. In Sec. 2, we give an overview of the current knowledge on the heavy-to-light transition form factors. The process $\overline{B}_s \rightarrow K^+ \ell \bar{\nu}$ will be discussed in Sec. 3, while the angular distributions for $\overline{B}_s \rightarrow K \pi \ell \bar{\nu}$ will be derived in Sec. 4. With these quantities we explore various distribution observables for $\overline{B}_s^0 \rightarrow K^0 \pi^+ \ell \bar{\nu}$ and $B^- \rightarrow \pi^+ \pi^- \ell \bar{\nu}$ including the differential decay widths, the S-wave fraction, and the forward-backward asymmetry. We summarise our findings in Sec. 5. Some detailed expressions for the angular coefficients are relegated to the Appendix.

2 Form factors

After integrating out the virtual W -boson, we arrive at the effective Hamiltonian describing the $b \rightarrow u$ transition

$$\mathcal{H}_{eff} = \frac{G_F}{\sqrt{2}} V_{ub} [\bar{u} \gamma_\mu (1 - \gamma_5) b] [\bar{\ell} \gamma^\mu (1 - \gamma_5) \nu] + h.c., \quad (2.1)$$

with G_F the Fermi constant. The leptonic part is calculable using perturbation theory while the hadronic effects are encoded in the transition form factors,

$$\langle K^+(p_2) | \bar{u} \gamma_\mu b | \bar{B}_s(p_B) \rangle = F_+^{\bar{B}_s \rightarrow K}(q^2) \left(P_\mu - \frac{m_{B_s}^2 - m_K^2}{q^2} q_\mu \right) + F_0^{\bar{B}_s \rightarrow K}(q^2) \frac{m_{B_s}^2 - m_K^2}{q^2} q_\mu, \quad (2.2)$$

with $q = p_B - p_2$, and $P = p_B + p_2$. In this $\bar{B}_s \rightarrow K^+$ transition, the strange quark serves as a spectator. As we will show in the following, the parametrization of the form factors for higher resonances with relatively small widths are also needed in the reactions $\bar{B}_s^0 \rightarrow K^0 \pi^+ \ell \bar{\nu}$. The decay $\bar{B}_s \rightarrow K_0^*$, where K_0^* is a scalar resonance, is described by

$$\begin{aligned} \langle K_0^{*+}(p_2) | \bar{u} \gamma_\mu \gamma_5 b | \bar{B}_s(p_B) \rangle = & -i \left\{ F_+^{\bar{B}_s \rightarrow K_0^*}(q^2) \left[P_\mu - \frac{m_{B_s}^2 - m_{K_0^*}^2}{q^2} q_\mu \right] \right. \\ & \left. + F_0^{\bar{B}_s \rightarrow K_0^*}(q^2) \frac{m_{B_s}^2 - m_{K_0^*}^2}{q^2} q_\mu \right\}, \end{aligned} \quad (2.3)$$

while the $\bar{B}_s \rightarrow K_J^*$ form factors with $J \geq 1$ are defined by [50–52]

$$\begin{aligned} \langle K_J^*(p_2, \epsilon) | \bar{u} \gamma^\mu b | \bar{B}_s(p_B) \rangle = & -\frac{2V(q^2)}{m_{B_s} + m_{K_J^*}} \epsilon^{\mu\nu\rho\sigma} \epsilon_{J\nu}^* P_{B\rho} P_{2\sigma}, \\ \langle K_J^*(p_2, \epsilon) | \bar{u} \gamma^\mu \gamma_5 b | \bar{B}_s(p_B) \rangle = & 2im_{K_J^*} A_0(q^2) \frac{\epsilon_J^* \cdot q}{q^2} q^\mu + i(m_{B_s} + m_{K_J^*}) A_1(q^2) \left[\epsilon_{J\mu}^* - \frac{\epsilon_J^* \cdot q}{q^2} q^\mu \right] \\ & - iA_2(q^2) \frac{\epsilon_J^* \cdot q}{m_{B_s} + m_{K_J^*}} \left[P^\mu - \frac{m_{B_s}^2 - m_{K_J^*}^2}{q^2} q^\mu \right]. \end{aligned} \quad (2.4)$$

We have adopted the convention $\epsilon^{0123} = +1$, and the polarisation vector in the above equations is constructed from the rank J polarisation tensor

$$\epsilon_{J\mu}(h) = \frac{1}{m_{B_s}^{J-1}} \epsilon_{\mu\nu_1\nu_2\dots\nu_{J-1}}(h) p_{B_s}^{\nu_1} p_{B_s}^{\nu_2} \dots p_{B_s}^{\nu_{J-1}}, \quad (2.5)$$

with the helicity $h = 0, \pm 1$. In the case $J = 1$, $\epsilon_{J\mu} = \epsilon_\mu$.

For the $B_s \rightarrow K$ transition form factor, no published result is available from LQCD simulations, though some preliminary results can be found in Ref. [53]. The QCD sum rules results from Ref. [54] do not provide the analytic information to access the q^2 distribution of the form factors. In this work, our following calculation relies on some QCD-motivated models [9–12] and the factorisation approach [8]. For the momentum-transfer distribution,

Table 1. Theoretical predictions of the $B_s \rightarrow K$ transitions form factors, in the light-front quark model (LFQM), relativistic quark model (RQM) and the perturbative QCD approach (PQCD).

	$F_1(0)$	a_{F_1}	b_{F_1}	$F_0(0)$	a_{F_0}	b_{F_0}
LFQM [12]	0.23 ± 0.01	1.88	1.58	0.23 ± 0.01	1.05	0.35
PQCD [8]	0.26 ± 0.06	0.57	0.50	0.26 ± 0.06	0.54	-0.15
RQM [9]	0.284 ± 0.014	-0.37	-1.41	0.284 ± 0.014	-0.072	-0.651

the most intuitive and simplest parametrization of the $B_s \rightarrow K$ form factors is the dipole form:

$$F_i^{B_s \rightarrow K}(q^2) = \frac{F_i^{B_s \rightarrow K}(0)}{(1 - aq^2/m_{B_s}^2 + bq^4/m_{B_s}^4)}, \quad (2.6)$$

which has been widely used in the light-front quark model (LFQM) [10–12]. In a recent calculation based on a relativistic quark model (RQM) [9], the q^2 -dependence of the form factors is parametrized as

$$\begin{aligned} F_1^{B_s \rightarrow K}(q^2) &= \frac{F_1^{B_s \rightarrow K}(0)}{(1 - q^2/m_B^2)(1 - aq^2/m_{B^*}^2 + bq^4/m_{B^*}^4)}, \\ F_0^{B_s \rightarrow K}(q^2) &= \frac{F_0^{B_s \rightarrow K}(0)}{(1 - aq^2/m_{B^*}^2 + bq^4/m_{B^*}^4)}. \end{aligned} \quad (2.7)$$

The perturbative QCD (PQCD) calculation [8] based on the k_T -factorisation [55–58] at next-to-leading order in α_s [59] yields:

$$\begin{aligned} F_1^{B_s \rightarrow K}(q^2) &= F_1^{B_s \rightarrow K}(0) \left(\frac{1}{(1 - q^2/m_{B_s}^2)} + \frac{aq^2/m_{B_s}^2}{(1 - q^2/m_{B_s}^2)(1 - bq^2/m_{B_s}^2)} \right), \\ F_0^{B_s \rightarrow K}(q^2) &= \frac{F_0^{B_s \rightarrow K}(0)}{(1 - aq^2/m_{B_s}^2 + bq^4/m_{B_s}^4)}. \end{aligned} \quad (2.8)$$

Results for these inputs from Refs. [8, 9, 12] are collected in Tab. 1, where for the LFQM results, we have also introduced the parametric uncertainties as done in Ref. [60–62].

For $B_s \rightarrow K^*$, we use the results from the recent Lattice QCD simulation [6] and the LCSR [7] as the central inputs. The LQCD calculation has used the following parametrization to describe the q^2 -dependence:

$$F(q^2) = \frac{1}{P(q^2, \Delta m)} [a_0 + a_1 z], \quad (2.9)$$

with

$$\begin{aligned} z &= \frac{\sqrt{t_+ - t} - \sqrt{t_+ - t_0}}{\sqrt{t_+ - t} + \sqrt{t_+ - t_0}}, \\ t_{\pm} &= (m_{B_s} \pm m_{K^*})^2, \quad t_0 = 12 \text{ GeV}^2, \\ P(q^2, \Delta m) &= 1 - \frac{q^2}{(m_{B_s} + \Delta m)^2}. \end{aligned} \quad (2.10)$$

Table 2. The $B_s \rightarrow K^*$ transitions form factors from the LCSR [7] and Lattice QCD [6], for the $B \rightarrow \rho$ transition, we quote the LCSR [7] and LFQM [10] results.

LQCD [6]	Δm (MeV)	a_0	a_1		
$V^{B_s \rightarrow K^*}$	-42	0.321 ± 0.048	-3.04 ± 0.68		
$A_0^{B_s \rightarrow K^*}$	-87	0.473 ± 0.042	-2.28 ± 0.74		
$A_1^{B_s \rightarrow K^*}$	350	0.2337 ± 0.0116	0.082 ± 0.133		
$A_{12}^{B_s \rightarrow K^*}$	350	0.1919 ± 0.0130	0.376 ± 0.191		
LCSR [7]	$F(0)$	r_1	m_R^2	r_2	m_{fit}^2
$V^{B_q \rightarrow \rho}$	0.323 ± 0.030	1.045	5.32^2	-0.721	38.34
$A_0^{B_q \rightarrow \rho}$	0.303 ± 0.029	1.527	5.28^2	-1.220	33.36
$A_1^{B_q \rightarrow \rho}$	0.242 ± 0.023			0.240	37.51
$A_2^{B_q \rightarrow \rho}$	0.221 ± 0.023	0.009		0.212	40.82
$V^{B_s \rightarrow K^*}$	0.311 ± 0.026	2.351	5.42^2	-2.039	33.10
$A_0^{B_s \rightarrow K^*}$	0.360 ± 0.034	2.813	5.37^2	-2.509	31.58
$A_1^{B_s \rightarrow K^*}$	0.233 ± 0.022			0.231	32.94
$A_2^{B_s \rightarrow K^*}$	0.181 ± 0.025	-0.011		0.192	40.14
LFQM [10]	F_0	a	b		
$V^{B \rightarrow \rho}$	0.27	1.84	1.28		
$A_0^{B \rightarrow \rho}$	0.28	1.73	1.20		
$A_1^{B \rightarrow \rho}$	0.22	0.95	0.21		
$A_2^{B \rightarrow \rho^*}$	0.20	1.65	1.05		

To access the quantity A_2 , in the LQCD simulation an auxiliary function was calculated:

$$A_{12}(q^2) = \frac{(m_B + m_V)^2(m_B^2 - m_V^2 - q^2)A_1(q^2) - (t_+ - t)(t_- - t)A_2(q^2)}{16m_b m_V^2(m_B + m_V)}, \quad (2.11)$$

which improves the numerical stability. In the LCSR [7], the form factors are parametrized as

$$\begin{aligned} V(q^2)/A_0(q^2) &= \frac{r_1}{1 - q^2/m_R^2} + \frac{r_2}{1 - q^2/m_{\text{fit}}^2} \\ A_1(q^2) &= \frac{r_2}{1 - q^2/m_{\text{fit}}^2}, \\ A_0(q^2) &= \frac{r_1}{1 - q^2/m_{\text{fit}}^2} + \frac{r_2}{(1 - q^2/m_{\text{fit}}^2)^2}. \end{aligned} \quad (2.12)$$

The results for these inputs are shown in Tab. 2. The differences caused by these form factors reflect the systematic uncertainties.

In the region where the two pseudo-scalar mesons strongly interact, the resonance approximation fails and thus has to be abandoned. One of the such examples is the S-wave

Table 3. Theoretical results for the $B_s \rightarrow \kappa$ and $B \rightarrow \sigma$ form factors in the perturbative QCD approach [69] with the parametrization given in Eq. (2.6).

	$F_1(0)$	a_{F_1}	b_{F_1}	$F_0(0)$	a_{F_0}	b_{F_0}
$B_s \rightarrow \kappa$	0.29 ± 0.07	1.62	0.56	0.29 ± 0.07	1.68	0.62
$B \rightarrow \sigma$	0.28 ± 0.07	1.61	0.56	0.28 ± 0.07	0.65	-0.11

below 1 GeV, for which we can use the form factors as defined in Ref. [15]:

$$\begin{aligned} \langle (K\pi)_0(p_{K\pi}) | \bar{u}\gamma_\mu\gamma_5 b | \bar{B}_s(p_B) \rangle = & -i \frac{1}{m_{K\pi}} \left\{ \left[P_\mu - \frac{m_{B_s}^2 - m_{K\pi}^2}{q^2} q_\mu \right] \mathcal{F}_1^{B_s \rightarrow K\pi}(m_{K\pi}^2, q^2) \right. \\ & \left. + \frac{m_{B_s}^2 - m_{K\pi}^2}{q^2} q_\mu \mathcal{F}_0^{B_s \rightarrow K\pi}(m_{K\pi}^2, q^2) \right\}. \end{aligned} \quad (2.13)$$

Watson's theorem implies that the phases measured in $K\pi$ elastic scattering and in a decay channel in which the $K\pi$ system has no strong interaction with other hadrons are equal (modulo π). In the process we consider here, the lepton pair $\ell\bar{\nu}$ indeed decouples from the $K\pi$ final state, and thus we have

$$\langle (K\pi)_0 | \bar{u}\Gamma b | \bar{B}_s \rangle \propto F_{K\pi}(m_{K\pi}^2), \quad (2.14)$$

where the strangeness-changing scalar form factors are defined by

$$\langle 0 | \bar{s}d | K\pi \rangle = C_X \frac{m_K^2 - m_\pi^2}{m_s - m_d} F_{K\pi}(m_{K\pi}^2). \quad (2.15)$$

Here C_X is an isospin factor. In the following, we will consider $K^0\pi^+$ with $C_X = 1$, and the $K^+\pi^0$ channel is similar.

It is worthwhile to point out that the generalized form factors also affect charmless three-body nonleptonic B -decays under the factorisation assumption, see e.g. [63–65]. An explicit calculation of these quantities [66], requires the knowledge of generalised light-cone distribution amplitudes [67]. The twist-3 one has the same asymptotic form as the distribution amplitudes for a scalar resonance [68]. Inspired by this similarity, we introduce an intuitive matching:

$$\mathcal{F}_i^{B_s \rightarrow K\pi}(m_{K\pi}^2, q^2) = \frac{m_K^2 - m_\pi^2}{m_s - m_u} \frac{1}{f_\kappa} F_{K\pi}(m_{K\pi}^2) F_i^{B_s \rightarrow \kappa}(q^2), \quad (2.16)$$

where the $B_s \rightarrow \kappa$ form factors have been calculated in the PQCD approach [69]. For the $B^- \rightarrow \pi^+\pi^-\ell\bar{\nu}$ form factors, we refer the reader to the scalar $\pi\pi$ form factors in Refs. [37, 72] that combine unitarization methods and chiral perturbation theory. Further, we use the $B \rightarrow \sigma$ form factors induced by the $b \rightarrow u$ transition from Ref. [69] which are collected in Tab. 3. Using the $B \rightarrow f_0(980)$ form factors which are also generated by the $b \rightarrow u$ transition, would enhance the results on the S-wave contributions given in the following by a factor $0.39^2/0.28^2 \simeq 1.9$ [69].

3 $B_s \rightarrow K \ell \bar{\nu}_\ell$

With the form factors defined in Eq. (2.2), we evaluate the $B_s \rightarrow K$ matrix elements as

$$H_0 = \frac{G_F}{\sqrt{2}} V_{ub} \frac{\sqrt{\lambda}}{\sqrt{q^2}} F_1^{B_s \rightarrow K}(q^2), \quad H_t = \frac{G_F}{\sqrt{2}} V_{ub} \frac{m_{B_s}^2 - m_K^2}{\sqrt{q^2}} F_0^{B_s \rightarrow K}(q^2), \quad (3.1)$$

and obtain the differential decay rate for $\bar{B}_s^0 \rightarrow K^+ \ell \bar{\nu}_\ell$ as a function of q^2 and θ_l

$$\frac{d^2\Gamma(\bar{B}_s \rightarrow K^+ \ell^- \bar{\nu}_\ell)}{dq^2 d\cos\theta_l} = \frac{1}{512\pi^3 m_{B_s}^3} \sqrt{\lambda} 4q^2 \beta_l^2 [\sin^2\theta_l |H_0|^2 + \hat{m}_l^2 |H_t + H_0 \cos\theta_l|^2], \quad (3.2)$$

where $\beta_l = 1 - \hat{m}_l^2$, $\hat{m}_i = m_i/\sqrt{q^2}$ and $\lambda = \lambda(m_{B_s}^2, q^2, m_K^2)$ is the Källén function

$$\lambda(a, b, c) = a^2 + b^2 + c^2 - 2(ab + bc + ca). \quad (3.3)$$

Here, θ_l is defined as the polar angle of the lepton momentum relative to the moving direction of the B_s -meson in the q^2 rest frame. Integrating over the polar angle, the differential partial width in q^2 is given by

$$\frac{d\Gamma(\bar{B}_s \rightarrow K^+ \ell^- \bar{\nu}_\ell)}{dq^2} = \frac{1}{128\pi^3 m_{B_s}^3} \sqrt{\lambda} q^2 \beta_l^2 \left[\frac{4}{3} |H_0|^2 + 2\hat{m}_l^2 |H_t|^2 + \frac{2}{3} \hat{m}_l^2 |H_0|^2 \right]. \quad (3.4)$$

One can also explore the q^2 -dependent ratio

$$\mathcal{R}_K^{\tau/\mu}(q^2) = \frac{d\Gamma(\bar{B}_s \rightarrow K^+ \tau^- \bar{\nu}_\tau)/dq^2}{d\Gamma(\bar{B}_s \rightarrow K^+ \mu^- \bar{\nu}_\mu)/dq^2}, \quad (3.5)$$

and its integrated form:

$$R_K^{\tau/\mu} = \frac{\Gamma(\bar{B}_s \rightarrow K^+ \tau^- \bar{\nu}_\tau)}{\Gamma(\bar{B}_s \rightarrow K^+ \mu^- \bar{\nu}_\mu)}, \quad (3.6)$$

where the μ lepton can also be replaced by the electron. Using three sets of form factors, we show the results for the $\bar{B}_s \rightarrow K^+ \ell^- \bar{\nu}_\ell$ differential decay widths $d\Gamma/dq^2/|V_{ub}|^2$ (in units of $1/(\text{ps} \times \text{GeV}^2)$) in Fig. 1, with $\ell = \mu, e$ in the first panel and $\ell = \tau$ in the second panel. The ratio $R_K^{\tau/\mu}(q^2)$ is also given in the last panel. The solid, dashed and dotted curves correspond to the form factors calculated from the RQM, LFQM and PQCD approaches. Errors caused by the input parameters in the $R_K^{\tau/\mu}(q^2)$ mostly cancel in the three individual sets of calculations, but distributions are quite different especially in the large q^2 region.

Since the differential decay rate in Eq. (3.2) involves the polar angle of the lepton, we can define an angular asymmetry:

$$\mathcal{A}_{FB}^K(q^2) = \left[\int_0^1 - \int_{-1}^0 \right] d\cos\theta_l \frac{d^2\Gamma(\bar{B}_s \rightarrow K^+ \ell^- \bar{\nu}_\ell)}{dq^2 d\cos\theta_l}. \quad (3.7)$$

More explicitly, the normalised asymmetry for $\bar{B}_s \rightarrow K \ell \bar{\nu}_\ell$ decay is given by

$$\bar{\mathcal{A}}_{FB}^K(q^2) = \frac{\mathcal{A}_{FB}^K(q^2)}{d\Gamma/dq^2} = \frac{2\hat{m}_l^2 \text{Re}[H_0 H_t^*]}{(4/3 + 2/3\hat{m}_l^2) |H_0|^2 + 2\hat{m}_l^2 |H_t|^2}. \quad (3.8)$$

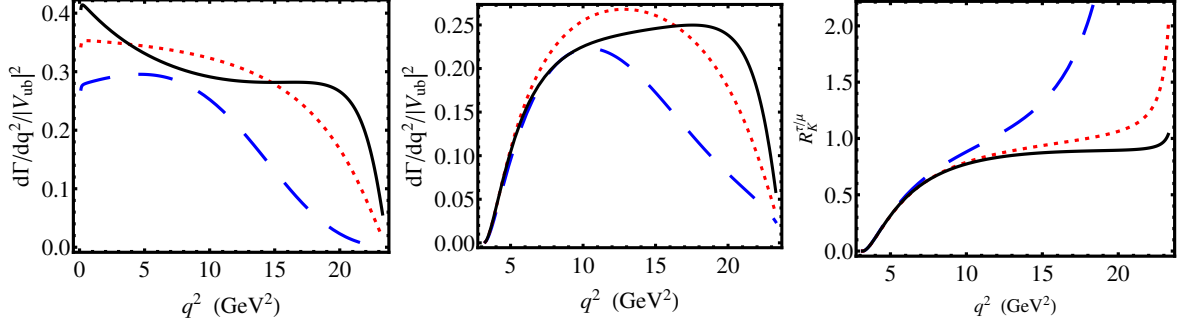


Figure 1. Differential decay widths (in units of $1/(\text{ps} \times \text{GeV}^2)$) for $\bar{B}_s^0 \rightarrow K^+ \ell \bar{\nu}_\ell$ with $\ell = \mu, e$ in the first panel and $\ell = \tau$ in the second panel. The q^2 -dependent ratio $R_K^{\tau/\mu}$ defined in Eq. (3.5) is given in the last panel. The solid, dashed and dotted curves correspond to the form factors calculated using the RQM, LFQM and PQCD approachess, respectively.

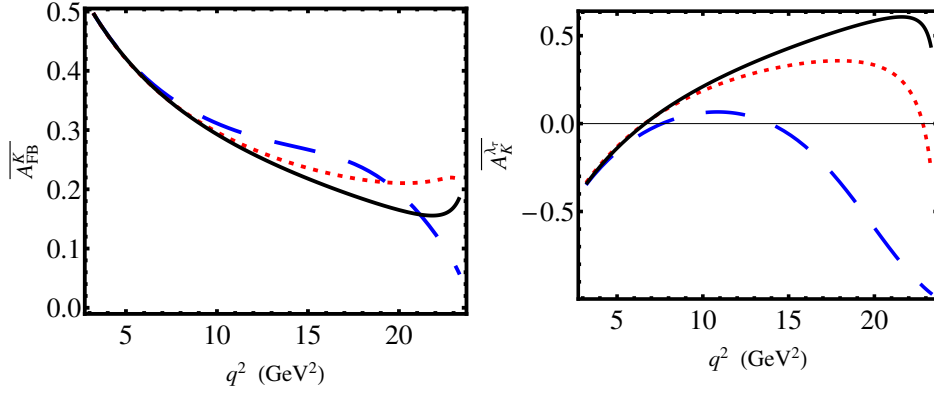


Figure 2. Same as Fig. 1 but for the forward-backward asymmetry (the left panel) defined in Eq. (3.7), and the polarisation fraction for the τ lepton (the right panel).

Clearly, the angular asymmetry is only associated with the ratio of form factors, which supposedly is less sensitive to the model-dependent hadronic parameters. Therefore, this quantity could be a good candidate to explore the new physics effects.

The lepton is produced from the $V - A$ current in the SM, and thus the lepton and muon is mainly left-handed polarised. For the τ lepton, we can also explore the polarised distribution,

$$\begin{aligned} \frac{d^2\Gamma(\bar{B}_s \rightarrow K^+ \tau^- \bar{\nu}_\tau(\lambda_\tau = -1/2))}{dq^2 d\cos\theta_l} &= \frac{1}{128\pi^3 m_{B_s}^3} \sqrt{\lambda} q^2 \beta_l^2 \sin^2\theta |H_0|^2, \\ \frac{d^2\Gamma(\bar{B}_s \rightarrow K^+ \tau^- \bar{\nu}_\tau(\lambda_\tau = 1/2))}{dq^2 d\cos\theta_l} &= \frac{1}{128\pi^3 m_{B_s}^3} \sqrt{\lambda} q^2 \beta_l^2 \hat{m}_l^2 |H_t + H_0 \cos\theta|^2, \end{aligned} \quad (3.9)$$

Table 4. Integrated decay widths for $B_s \rightarrow K^+ \ell \bar{\nu}$: $\Delta\zeta_K^\ell(q_l^2, q_u^2)$. Results are given in units of ps^{-1} .

	LFQM	PQCD	RQM
$\Delta\zeta_K^\mu(0, 4)$	1.12 ± 0.099	1.36 ± 0.703	1.47 ± 0.149
$\Delta\zeta_K^\mu(4, 8)$	1.17 ± 0.099	1.36 ± 0.702	1.28 ± 0.135
$\Delta\zeta_K^\mu(8, 12)$	$1. \pm 0.089$	1.29 ± 0.664	1.17 ± 0.116
$\Delta\zeta_K^\mu(0, 23.77)$	4.18 ± 0.372	6.38 ± 3.29	6.83 ± 0.688
$\Delta\zeta_K^\tau(m_\tau^2, 8)$	0.551 ± 0.049	0.614 ± 0.317	0.577 ± 0.058
$\Delta\zeta_K^\tau(8, 12)$	0.872 ± 0.077	1.01 ± 0.516	0.894 ± 0.09
$\Delta\zeta_K^\tau(m_\tau^2, 23.77)$	2.82 ± 0.25	3.95 ± 2.03	4.04 ± 0.406
$R_K^{\tau/\mu}$	0.675	0.619	0.592

and the polarisation fraction:

$$\begin{aligned} \bar{A}_K^{\lambda_\tau}(q^2) &= \frac{d\Gamma(\bar{B}_s \rightarrow K^+ \tau^- \bar{\nu}_\tau)(\lambda_\tau = -1/2)/dq^2 - d\Gamma(\bar{B}_s \rightarrow K^+ \tau^- \bar{\nu}_\tau)(\lambda_\tau = 1/2)/dq^2}{d\Gamma(\bar{B}_s \rightarrow K^+ \tau^- \bar{\nu}_\tau)/dq^2} \\ &= \frac{(4/3 - 2/3\hat{m}_l^2)|H_0|^2 - 2\hat{m}_l^2|H_t|^2}{(4/3 + 2/3\hat{m}_l^2)|H_0|^2 + 2\hat{m}_l^2|H_t|^2}. \end{aligned} \quad (3.10)$$

Results for the asymmetries and polarisations are given in Fig. 2, where different theoretical calculations of form factors lead to different behaviours especially in the large q^2 (low recoil) region. This can be improved once the Lattice QCD can constrain the form factors. In this procedure, we also notice that Lattice QCD simulation often requests an extrapolation from the unrealistic quark mass region to physical region. The hard pion chiral perturbation theory approach advocated in Refs. [70, 71] has the advantage to resum the chiral logarithms and thus are valuable for the extrapolation. Such effects should be taken into account in the future Lattice QCD simulation.

The integrated decay widths in terms of $|V_{ub}|^2$ are given in Tab. 4, with the definition

$$\Delta\zeta_K^\ell(q_l^2, q_u^2) = \frac{1}{|V_{ub}|^2} \int_{q_l^2}^{q_u^2} dq^2 \frac{d\Gamma(\bar{B}_s \rightarrow K^+ \ell \bar{\nu})}{dq^2}. \quad (3.11)$$

These values will be useful to extract the $|V_{ub}|$ when compared to the experimental data available in future. The PQCD approach gives the largest errors due to the uncertainties in the form factors, while the other approaches have approximately 10% parametric errors.

4 Full angular distribution of $B_s \rightarrow K\pi\ell\bar{\nu}$

We consider the kinematics for the $B_s \rightarrow K\pi\ell\bar{\nu}$ as shown in Fig. 3. The $K\pi$ system moves along the z -axis in the \bar{B}_s rest-frame. $\theta_K(\theta_l)$ is defined in the $K\pi$ (lepton pair) rest frame as the angle between z -axis and the direction of motion of the K (ℓ^-), respectively. The azimuth angle ϕ is the relative angle between the $K\pi$ decay and lepton pair planes.

The decay amplitudes for $B_s \rightarrow K\pi\ell\bar{\nu}$ can be divided into several individual pieces and each of them can be expressed in terms of the Lorentz invariant helicity amplitudes.

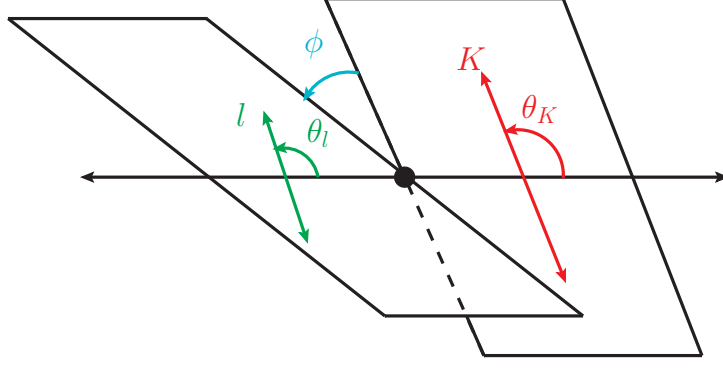


Figure 3. Kinematics for $\overline{B}_s \rightarrow K\pi\ell\bar{\nu}$. The $K\pi$ system moves along the z axis in the \overline{B}_s rest frame. $\theta_K(\theta_l)$ is defined in the $K\pi$ (lepton pair) rest-frame as the angle between the z -axis and the direction of motion of the K (ℓ^-), respectively. The azimuth angle ϕ is the relative angle between the $K\pi$ decay and lepton pair planes.

The amplitude for the hadronic part can be obtained from the matrix element:

$$A_\lambda = \sqrt{N_{K_J^*}} \frac{iG_F}{\sqrt{2}} V_{ub} \epsilon_\mu^*(h) \langle K\pi | \bar{u} \gamma^\mu (1 - \gamma_5) b | \overline{B}_s \rangle, \quad (4.1)$$

where $\epsilon_\mu(h)$ is an auxiliary polarisation vector for the lepton pair system, $h = 0, \pm, t$, and $N_{K_J^*} = \sqrt{\lambda} q^2 \beta_l / (96\pi^3 m_{B_s}^3)$. The functions A_i can be decomposed into different partial-waves

$$\begin{aligned} A_{0/t}(q^2, m_{K\pi}^2, \theta_K) &= \sum_{J=0,1,2,\dots} A_{0/t}^J(q^2, m_{K\pi}^2) Y_J^0(\theta_K, 0), \\ A_{||/\perp}(q^2, m_{K\pi}^2, \theta_K) &= \sum_{J=0,1,2,\dots} A_{||/\perp}^J(q^2, m_{K\pi}^2) Y_J^{-1}(\theta, 0), \\ A_i^J(q^2, m_{K\pi}^2) &= \sqrt{N_{K_J^*}} \mathcal{M}_B(K_J^*, i)(q^2) L_{K_J^*}(m_{K\pi}^2) \equiv |A_i^J| e^{i\delta_i^J}. \end{aligned} \quad (4.2)$$

Here, the subscript t denotes the time-like component of a virtual vector/axial-vector meson that decays into the lepton pair. $L_{K_J^*}(m_{K\pi})$ is the lineshape, and for the P-wave resonance $K^*(892)$, we use the Breit-Wigner distribution:

$$L_{K^*}(m_{K\pi}^2) = \sqrt{\frac{m_{K^*} \Gamma_{K^* \rightarrow K\pi}}{\pi}} \frac{1}{m_{K\pi}^2 - m_{K^*}^2 + im_{K^*} \Gamma_{K^*}}. \quad (4.3)$$

Considering the momentum dependence of the K^* decay, we have the running width

$$\Gamma_{K^*}(m_{K\pi}^2) = \Gamma_{K^*}^0 \left(\frac{|\vec{q}|}{|\vec{q}_0|} \right)^3 \frac{m_{K^*}}{m_{K\pi}} \frac{1 + (R|\vec{q}_0|)^2}{1 + (R|\vec{q}|)^2}, \quad (4.4)$$

and the Blatt-Weisskopf parameter $R = (2.1 \pm 0.5 \pm 0.5) \text{GeV}^{-1}$ [73]. In the following, we will suppress the dependence on the $q^2, m_{K\pi}$, and the polar angle θ_K for simplicity.

The spin-0 final state has only one polarisation state and the amplitudes are

$$i\mathcal{M}_B(K_0^*, 0) = N_1 i \left[\frac{\sqrt{\lambda}}{\sqrt{q^2}} F_1(q^2) \right], \quad i\mathcal{M}_B(K_0^*, t) = N_1 i \left[\frac{m_{B_s}^2 - m_{K_0^*}^2}{\sqrt{q^2}} F_0(q^2) \right], \quad (4.5)$$

with $N_1 = iG_F V_{ub}/\sqrt{2}$. In the case of strange mesons with spin $J \geq 1$, the $K^-\pi^+$ system can be either longitudinally or transversely polarised and thus we have the following form:

$$i\mathcal{M}_B(K_J^*, 0) = \frac{\alpha_L^J N_1 i}{2m_{K_J^*} \sqrt{q^2}} \left[(m_{B_s}^2 - m_{K_J^*}^2 - q^2)(m_{B_s} + m_{K_J^*}) A_1 - \frac{\lambda}{m_{B_s} + m_{K_J^*}} A_2 \right],$$

$$i\mathcal{M}_B(K_J^*, \pm) = \beta_T^J N_1 i \left[(m_{B_s} + m_{K_J^*}) A_1 \mp \frac{\sqrt{\lambda}}{m_{B_s} + m_{K_J^*}} V \right], \quad (4.6)$$

$$i\mathcal{M}_B(K_J^*, L, t) = \alpha_L^J i N_1 \frac{\sqrt{\lambda}}{\sqrt{q^2}} A_0. \quad (4.7)$$

Here, α_L^J and β_T^J are products of the Clebsch-Gordan coefficients

$$\alpha_L^J = C_{1,0;J-1,0}^{J,0} C_{1,0;J-2,0}^{J-1,0} \dots C_{1,0;1,0}^{2,0}, \quad \beta_T^J = C_{1,1;J-1,0}^{J,1} C_{1,0;J-2,0}^{J-1,0} \dots C_{1,0;1,0}^{2,0}. \quad (4.8)$$

For the sake of convenience, we can define

$$i\mathcal{M}_B(K_J^*, \perp / ||) = \frac{1}{\sqrt{2}} [i\mathcal{M}_B(K_J^*, +) \mp i\mathcal{M}_B(K_J^*, -)],$$

$$i\mathcal{M}_B(K_J^*, \perp) = -i\beta_T^J \sqrt{2} N_1 \left[\frac{\sqrt{\lambda} V}{m_{B_s} + m_{K_J^*}} \right],$$

$$i\mathcal{M}_B(K_J^*, ||) = i\beta_T^J \sqrt{2} N_1 \left[(m_{B_s} + m_{K_J^*}) A_1 \right]. \quad (4.9)$$

Using the generalised form factor, the matrix elements for B_s decays into the spin-0 non-resonating $K\pi$ final state are given as

$$A_0^0 = \sqrt{N_2} i \frac{1}{m_{K\pi}} \left[\frac{\sqrt{\lambda}}{\sqrt{q^2}} \mathcal{F}_1^{B_s \rightarrow K\pi}(m_{K\pi}^2, q^2) \right] \equiv \sqrt{N_{K_J^*}} L_S(m_{K\pi}^2) i \left[\frac{\sqrt{\lambda}}{\sqrt{q^2}} F_1^{B_s \rightarrow \kappa}(q^2) \right],$$

$$A_t^0 = \sqrt{N_2} i \frac{1}{m_{K\pi}} \left[\frac{m_{B_s}^2 - m_{K\pi}^2}{\sqrt{q^2}} \mathcal{F}_0^{B_s \rightarrow K\pi}(m_{K\pi}^2, q^2) \right]$$

$$\equiv \sqrt{N_{K_J^*}} L_S(m_{K\pi}^2) i \left[\frac{m_{B_s}^2 - m_{K\pi}^2}{\sqrt{q^2}} F_0^{B_s \rightarrow \kappa}(m_{K\pi}^2, q^2) \right], \quad (4.10)$$

where we have introduced a lineshape for the S-wave contribution. Here $N_2 = N_1 N_{K_J^*} \rho_K / (16\pi^2)$, and $\rho_K = \sqrt{[m_{K\pi}^2 - (m_K + m_\pi)^2][m_{K\pi}^2 - (m_K - m_\pi)^2]} / (m_{K\pi}^2)$.

The quantities given above lead to the full angular distributions

$$\begin{aligned} \frac{d^5\Gamma}{dm_{K\pi}^2 dq^2 d\cos\theta_K d\cos\theta_l d\phi} = & \frac{3}{8} \left[I_1(q^2, m_{K\pi}^2, \theta_K) \right. \\ & + I_2(q^2, m_{K\pi}^2, \theta_K) \cos(2\theta_l) \\ & + I_3(q^2, m_{K\pi}^2, \theta_K) \sin^2\theta_l \cos(2\phi) \\ & + I_4(q^2, m_{K\pi}^2, \theta_K) \sin(2\theta_l) \cos\phi \\ & + I_5(q^2, m_{K\pi}^2, \theta_K) \sin(\theta_l) \cos\phi \\ & + I_6(q^2, m_{K\pi}^2, \theta_K) \cos\theta_l \\ & + I_7(q^2, m_{K\pi}^2, \theta_K) \sin(\theta_l) \sin\phi \\ & + I_8(q^2, m_{K\pi}^2, \theta_K) \sin(2\theta_l) \sin\phi \\ & \left. + I_9(q^2, m_{K\pi}^2, \theta_K) \sin^2\theta_l \sin(2\phi) \right], \end{aligned} \quad (4.11)$$

with the I_i having the form:

$$\begin{aligned} I_1 &= (1 + \hat{m}_l^2)|A_0|^2 + 2\hat{m}_l^2|A_t|^2 + \frac{1}{2}(3 + \hat{m}_l^2)(|A_\perp|^2 + |A_\parallel|^2) \\ I_2 &= -\beta_l|A_0|^2 + \frac{1}{2}\beta_l^2(|A_\perp|^2 + |A_\parallel|^2), \\ I_3 &= \beta_l(|A_\perp|^2 - |A_\parallel|^2), \quad I_4 = 2\beta_l[\text{Re}(A_0 A_\parallel^*)], \\ I_5 &= 4[\text{Re}(A_0 A_\perp^*) - \hat{m}_l^2 \text{Re}(A_t A_\parallel^*)], \quad I_6 = 4[\text{Re}(A_\parallel A_\perp^*) + \hat{m}_l^2 \text{Re}(A_t A_0^*)], \\ I_7 &= 4[\text{Im}(A_0 A_\parallel^*) - \hat{m}_l^2 \text{Im}(A_t A_\perp^*)], \quad I_8 = 2\beta_l[\text{Im}(A_0 A_\perp^*)], \\ I_9 &= 2\beta_l[\text{Im}(A_\perp A_\parallel^*)]. \end{aligned} \quad (4.12)$$

For the general expressions of these functions, we refer the reader to the appendix, and also Ref. [24–26]. In the following, we shall only consider the S-wave and P-wave contributions and thus the above general expressions are reduced to:

$$\begin{aligned} I_1 &= \frac{1}{4\pi} [(1 + \hat{m}_l^2)|A_0^0|^2 + 2\hat{m}_l^2|A_t^0|^2] + \frac{3}{4\pi} \cos^2\theta_K [(1 + \hat{m}_l^2)|A_0^1|^2 + 2\hat{m}_l^2|A_t^1|^2] \\ &\quad + \frac{2\sqrt{3}\cos\theta_K}{4\pi} [(1 + \hat{m}_l^2)\text{Re}[A_0^0 A_0^{1*}] + 2\hat{m}_l^2 \text{Re}[A_t^0 A_t^{1*}]] \\ &\quad + \frac{3 + \hat{m}_l^2}{2} \frac{3}{8\pi} \sin^2\theta_K [|A_\perp^1|^2 + |A_\parallel^1|^2], \\ I_2 &= -\beta_l \left\{ \frac{1}{4\pi} |A_0^0|^2 + \frac{3}{4\pi} \cos^2\theta_K |A_0^1|^2 + \frac{2\sqrt{3}\cos\theta_K}{4\pi} \text{Re}[A_0^0 A_0^{1*}] \right\} \\ &\quad + \frac{1}{2}\beta_l \frac{3}{8\pi} \sin^2\theta_K (|A_\perp^1|^2 + |A_\parallel^1|^2), \\ I_3 &= \beta_l \frac{3}{8\pi} \sin^2\theta_K (|A_\perp^1|^2 - |A_\parallel^1|^2), \\ I_4 &= 2\beta_l \left[\frac{\sqrt{3}\sin\theta_K}{4\sqrt{2}\pi} \text{Re}[A_0^0 A_\parallel^{1*}] + \frac{3\sin\theta_K \cos\theta_K}{4\sqrt{2}\pi} \text{Re}[A_0^1 A_\parallel^{1*}] \right], \end{aligned}$$

$$\begin{aligned}
I_5 &= 4 \left\{ \frac{\sqrt{3} \sin \theta_K}{4\sqrt{2}\pi} (\text{Re}[A_0^0 A_{\perp}^{1*}] - \hat{m}_l^2 \text{Re}[A_t^0 A_{\parallel}^{1*}]) \right. \\
&\quad \left. + \frac{3 \sin \theta_K \cos \theta_K}{4\sqrt{2}\pi} (\text{Re}[A_0^1 A_{\perp}^{1*}] - \hat{m}_l^2 \text{Re}[A_t^1 A_{\parallel}^{1*}]) \right\}, \\
I_6 &= 4 \left\{ \frac{3}{8\pi} \sin^2 \theta_K \text{Re}[A_{\parallel}^1 A_{\perp}^{1*}] + \hat{m}_l^2 \frac{1}{4\pi} \text{Re}[A_t^0 A_0^{0*}] + \hat{m}_l^2 \frac{3}{4\pi} \cos^2 \theta_K \text{Re}[A_t^1 A_0^{1*}] \right\} \\
I_7 &= 4 \left\{ \frac{\sqrt{3}}{4\sqrt{2}\pi} \sin \theta_K (\text{Im}[A_0^0 A_{\parallel}^{1*}] - \hat{m}_l^2 \text{Im}[A_t^0 A_{\perp}^{1*}]) \right. \\
&\quad \left. + \frac{3}{4\sqrt{2}\pi} \sin \theta_K \cos \theta_K (\text{Im}[A_0^1 A_{\parallel}^{1*}] - \hat{m}_l^2 \text{Im}[A_t^1 A_{\perp}^{1*}]) \right\} \\
I_8 &= 2\beta_l \left\{ \frac{\sqrt{3}}{4\sqrt{2}\pi} \sin \theta_K \text{Im}[A_0^0 A_{\perp}^{1*}] + \frac{3}{4\sqrt{2}\pi} \sin \theta_K \cos \theta_K \text{Im}[A_0^1 A_{\perp}^{1*}] \right\}, \\
I_9 &= 2\beta_l \frac{3}{8\pi} \sin^2 \theta_K \text{Im}[A_{\perp}^1 A_{\parallel}^{1*}]. \tag{4.13}
\end{aligned}$$

One difference compared to the $B \rightarrow K\pi l^+ l^-$ distributions [14, 15], where the leptons have the same mass in the above coefficients, are: in $I_{5,6,7}$, the time component is present and interferes with the transverse polarisation. These are finite lepton mass corrections. Moreover, since the phase in the P-wave contributions arise from the line-shape which is the same for different polarisations, the I_9 term and the second line in the I_7 are zero here.

Measurements of the $B_s \rightarrow K\pi\ell\bar{\nu}$ and $B \rightarrow \pi\pi\ell\bar{\nu}$ processes can test the $\Delta I = 1/2$ rule [23, 26] since they are both induced by the $b \rightarrow u\ell\bar{\nu}$. However, channels with a neutral π^0 in the final state will request a high statistics to be accumulated in future experimental facilities.

These decay modes can also provide a probe for the T violation [23, 26]. As we have shown in the above, if only S-wave and P-wave are considered, the I_9 term and the second line in the I_7 are zero. These coefficients can be nonzero either due to the violation of T-invariance or higher partial-wave contribution. Furthermore, comparing the distributions for the B^- decay and its CP conjugation mode can examine the T-invariance as well, however it is difficult to generalize to the neutral B decays, since the B^0 and B_s^0 mix with their CP partner, respectively.

4.1 Differential and integrated decay widths

The starting point for a detailed analysis is to obtain the double-differential distribution $d^2\Gamma/dq^2/dm_{K\pi}^2$ after performing an integration over all the angles

$$\frac{d^2\Gamma}{dq^2 dm_{K\pi}^2} = \left(1 + \frac{\hat{m}_l^2}{2}\right) (|A_0^0|^2 + |A_0^1|^2 + |A_{\parallel}^1|^2 + |A_{\perp}^1|^2) + \frac{3}{2} \hat{m}_l^2 (|A_t^1|^2 + |A_t^0|^2), \tag{4.14}$$

where apparently in the massless limit for the involved lepton, the total normalization for the angular distributions changes to the sum of the S-wave and P-wave amplitudes

$$\frac{d^2\Gamma}{dq^2 dm_{K\pi}^2} = |A_0^0|^2 + |A_0^1|^2 + |A_{\parallel}^1|^2 + |A_{\perp}^1|^2. \tag{4.15}$$

To match the kinematics constraints implemented in the experimental measurements, one may explore the generic observable with $m_{K\pi}^2$ integrated out:

$$\langle O \rangle = \int_{(m_{K^*}-\delta_m)^2}^{(m_{K^*}+\delta_m)^2} dm_{K\pi}^2 \frac{dO}{dm_{K\pi}^2} . \quad (4.16)$$

Following the recent LHCb measurements on $B \rightarrow K^*(892)l^+l^-$ [74], we use the following choice in our study of $B_s \rightarrow K\pi\ell\bar{\nu}$:

$$\delta_m = 100\text{MeV}. \quad (4.17)$$

In the narrow width-limit for the P-wave contributions, the integration of the lineshape gives

$$\int dm_{K\pi}^2 |L_{K^*}(m_{K\pi}^2)|^2 = \mathcal{B}(K^{*+} \rightarrow K^0\pi^+) = \frac{2}{3} . \quad (4.18)$$

However with the explicit form given in Eq.(4.4), we find that the integration

$$\int_{(m_{K^*}-\delta_m)^2}^{(m_{K^*}+\delta_m)^2} dm_{K\pi}^2 |L_{K^*}(m_{K\pi}^2)|^2 = 0.56, \quad (4.19)$$

is below the expected value. This mismatch clearly indicates that one should be cautious to identify the experimental signal with theoretical results based on the purely P-wave contributions. On the other hand, the integrated S-wave lineshape in this region is

$$\int_{(m_{K^*}-\delta_m)^2}^{(m_{K^*}+\delta_m)^2} dm_{K\pi}^2 |L_S(m_{K\pi}^2)|^2 = 0.17, \quad (4.20)$$

which is at the same order and can not be neglected. Future experimental measurements should take this into account.

Furthermore, one may explore the q^2 -dependent ratio

$$R_{K\pi}^{\tau/\mu}(q^2) = \frac{\langle d\Gamma(\bar{B}_s \rightarrow K\pi\tau\bar{\nu})/dq^2 \rangle}{\langle d\Gamma(\bar{B}_s \rightarrow K\pi l\bar{\nu})/dq^2 \rangle}, \quad (4.21)$$

where l denotes the light lepton (e, μ). This ratio will be less sensitive to S-wave contributions.

Differential decay widths for $B_s \rightarrow K\pi\ell\bar{\nu}_\ell$ are given in Fig. 4, with $\ell = \mu, e$ and $\ell = \tau$ in the first two panels respectively. The q^2 -dependent ratio $R_{K\pi}^{\tau/\mu}$ as defined in Eq. (4.21) is given in the last panel.

Integrating over q^2 , one has the partial width

$$\Delta\zeta_{K\pi}^\ell(q_l^2, q_u^2) = \frac{1}{|V_{ub}|^2} \int_{q_l^2}^{q_u^2} dq^2 \left\langle \frac{d\Gamma}{dq^2} \right\rangle. \quad (4.22)$$

With the form factors from LQCD [6] and the LCSR [7], we give numerical results for $\Delta\zeta_{K^0\pi^+}^\ell(q_l^2, q_u^2)$ with different sets of q_l and q_u in Tab. 5. The S-wave contribution is calculated using the $K\pi$ scalar form factors and the $B_s \rightarrow \kappa$ transitions. Its contribution to the integrated partial widths ranges from 10% to approximately 20%. Since the S-wave contains the factor $1/\sqrt{q^2}$, as shown in Eq.(4.10), its contribution decreases with the increasing q^2 .

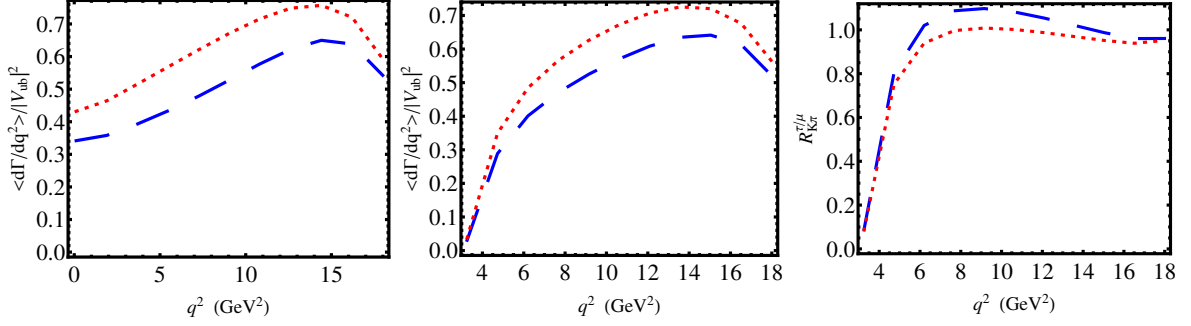


Figure 4. Differential decay widths (in units of $\text{ps}^{-1}\text{GeV}^{-2}$) for $\overline{B}_s \rightarrow K^0\pi^+\ell\bar{\nu}_\ell$ with $\ell = \mu, e$ in the first panel and $\ell = \tau$ in the second panel. The q^2 -dependent ratio $R_{K\pi}^{\tau/\mu}$ as defined in Eq. (4.21) is given in the last panel. The dashed and dotted curves are obtained using the LQCD and LCSR results for the $B_s \rightarrow K^*$ form factors.

Table 5. Integrated decay widths for $\overline{B}_s \rightarrow K^0\pi^+\ell\bar{\nu}$: $\Delta\zeta_{K\pi}^\ell(q_l^2, q_u^2)$. Results are given in units of ps^{-1} . The S-wave contributions are obtained with form factors calculated in the PQCD approach.

		S-Wave	P-Wave	Total	$f_S(\%)$
$\Delta\zeta_{K\pi}^\mu(0, 4)$	LQCD	0.278 ± 0.151	1.19 ± 0.151	1.47 ± 0.299	18.9
	LCSR	0.278 ± 0.151	1.61 ± 0.172	1.89 ± 0.321	14.7
$\Delta\zeta_{K\pi}^\mu(4, 8)$	LQCD	0.276 ± 0.149	1.58 ± 0.221	1.85 ± 0.376	14.9
	LCSR	0.276 ± 0.149	2.13 ± 0.296	2.41 ± 0.441	11.5
$\Delta\zeta_{K\pi}^\mu(8, 12)$	LQCD	0.254 ± 0.137	2.03 ± 0.305	2.29 ± 0.436	11.1
	LCSR	0.254 ± 0.137	2.6 ± 0.421	2.86 ± 0.552	8.88
$\Delta\zeta_{K\pi}^\mu(12, 16)$	LQCD	0.202 ± 0.109	2.43 ± 0.347	2.63 ± 0.458	7.68
	LCSR	0.202 ± 0.109	2.88 ± 0.505	3.08 ± 0.616	6.56
$\Delta\zeta_{K\pi}^\mu(0, 16)$	LQCD	1.01 ± 0.546	7.22 ± 1.03	8.23 ± 1.58	12.3
	LCSR	1.01 ± 0.546	9.23 ± 1.38	10.2 ± 1.97	9.9
$\Delta\zeta_{K\pi}^\tau(m_\tau^2, 8)$	LQCD	0.281 ± 0.152	1.36 ± 0.239	1.64 ± 0.392	17.1
	LCSR	0.281 ± 0.152	1.7 ± 0.253	1.98 ± 0.407	14.2
$\Delta\zeta_{K\pi}^\tau(8, 12)$	LQCD	0.299 ± 0.162	1.97 ± 0.319	2.27 ± 0.48	13.2
	LCSR	0.299 ± 0.162	2.38 ± 0.399	2.68 ± 0.56	11.2
$\Delta\zeta_{K\pi}^\tau(12, 16)$	LQCD	0.552 ± 0.299	4.32 ± 0.666	4.88 ± 0.958	11.3
	LCSR	0.552 ± 0.299	5.09 ± 0.873	5.64 ± 1.17	9.79
$\Delta\zeta_{K\pi}^\tau(m_\tau^2, 16)$	LQCD	0.834 ± 0.45	5.69 ± 0.895	6.52 ± 1.35	12.8
	LCSR	0.834 ± 0.45	6.78 ± 1.14	7.62 ± 1.58	10.9

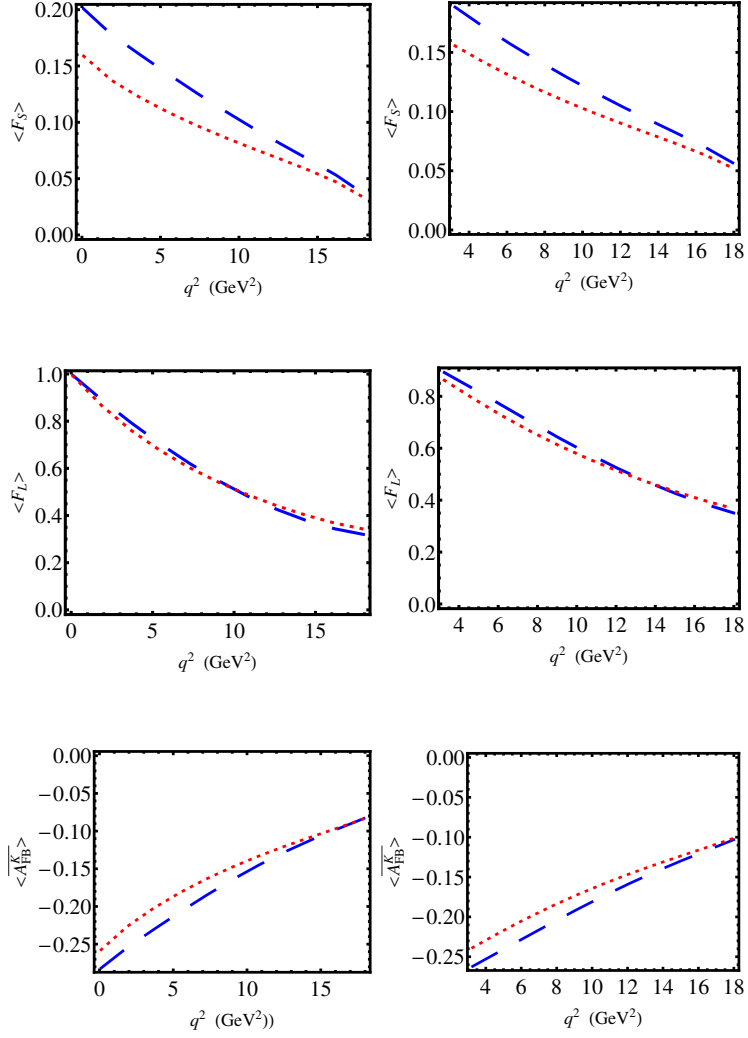


Figure 5. Same as Fig. 4 but for the S-wave contribution (a,b) and the longitudinal polarisations in the P-wave contribution (c,d) to the $B_s \rightarrow K\pi\ell\bar{\nu}_\ell$, and the forward-backward asymmetry $\overline{A_{FB}^K}$ (e,f). Notice that for $\overline{A_{FB}^K}$, there is a sign ambiguity arising from the use of the Watson theorem. The left panels are for the light lepton e, μ while the right panels are for the τ lepton.

4.2 Distribution in θ_K

We explore the distribution in θ_K :

$$\begin{aligned}
 \frac{d^3\Gamma}{dq^2 dm_{K\pi}^2 d\cos\theta_K} = \frac{1}{8} \bigg\{ & (4 + 2\hat{m}_l^2)|A_0^0|^2 + 6\hat{m}_l^2|A_t^0|^2 \\
 & + \sqrt{3}(8 + 4\hat{m}_l^2)\cos\theta_K \text{Re}[A_0^0 A_t^{1*}] + 12\sqrt{3}\hat{m}_l^2\cos\theta_K \text{Re}[A_t^0 A_t^{1*}] \\
 & + (12 + 6\hat{m}_l^2)|A_0^1|^2 \cos^2\theta_K + 18\hat{m}_l^2 \cos^2\theta_K |A_t^1|^2 \\
 & + (6 + 3\hat{m}_l^2)\sin^2\theta_K (|A_\perp^1|^2 + |A_\parallel^1|^2) \bigg\}. \quad (4.23)
 \end{aligned}$$

Compared to the distribution with only $B_s \rightarrow K^*(\rightarrow K\pi)\ell\bar{\nu}$, the first two lines of Eq. (4.23) are new: the first one is the S-wave $K\pi$ contribution, while the second line corresponds to the interference of S-wave and P-wave. Based on this interference, one can define a forward-backward asymmetry for the involved hadron,

$$\begin{aligned} A_{FB}^K &\equiv \left[\int_0^1 - \int_{-1}^0 \right] d\cos\theta_K \frac{d^3\Gamma}{dq^2 dm_{K\pi}^2 d\cos\theta_K} \\ &= \frac{\sqrt{3}}{2} (2 + \hat{m}_l^2) \text{Re}[A_0^0 A_0^{1*}] + \frac{3\sqrt{3}}{2} \hat{m}_l^2 \text{Re}[A_t^0 A_t^{1*}]. \end{aligned} \quad (4.24)$$

We define the polarisation fraction at a given value of q^2 and $m_{K\pi}^2$:

$$\begin{aligned} \mathcal{F}_S(q^2, m_{K\pi}^2) &= \frac{(1 + \hat{m}_l^2/2) |A_0^0|^2 + 3/2 \hat{m}_l^2 |A_t^0|^2}{d^2\Gamma/(dq^2 dm_{K\pi}^2)}, \\ \mathcal{F}_P(q^2, m_{K\pi}^2) &= \frac{(1 + \hat{m}_l^2/2) (|A_0^1|^2 + |A_{||}^1|^2 + |A_{\perp}^1|^2) + 3/2 |A_t^1|^2}{d^2\Gamma/(dq^2 dm_{K\pi}^2)}, \end{aligned} \quad (4.25)$$

and also

$$F_L(q^2, m_{K\pi}^2) = \frac{(1 + \hat{m}_l^2/2) (|A_0^1(q^2, m_{K\pi}^2)|^2 + 3/2 |A_t^1|^2)}{(1 + \hat{m}_l^2/2) (|A_0^1|^2 + |A_{||}^1|^2 + |A_{\perp}^1|^2) + 3/2 |A_t^1|^2}. \quad (4.26)$$

By definition, $\mathcal{F}_S + \mathcal{F}_P = 1$.

In Fig. 5. we give our results for the S-wave fraction $\langle F_S \rangle$, longitudinal polarisation fraction $\langle F_L \rangle$ in the P-wave contributions and the asymmetry $\langle A_{FB}^K \rangle$. The curves in the left panels are for the light lepton e, μ while the right three panels are for the τ lepton. These observables and the following ones are defined via the integration over $m_{K\pi}^2$, for instance

$$\langle F_S(q^2) \rangle = \frac{\int dm_{K\pi}^2 [(1 + \hat{m}_l^2/2) |A_0^0|^2 + 3/2 \hat{m}_l^2 |A_t^0|^2]}{\int dm_{K\pi}^2 d^2\Gamma/(dq^2 dm_{K\pi}^2)}, \quad (4.27)$$

and likewise for the others.

4.3 Distribution in θ_l and forward-backward asymmetry

After integrating over θ_K and ϕ , we have the distribution:

$$\begin{aligned} \frac{d^3\Gamma}{dq^2 dm_{K\pi}^2 d\cos\theta_l} &= \frac{3\pi}{4} \int d\cos\theta_K (I_1 + I_2 \cos(2\theta_l) + I_6 \cos\theta_l) \\ &= \frac{3}{4} \hat{m}_l^2 (|A_t^0|^2 + |A_t^1|^2) \\ &\quad + \frac{3}{2} \cos\theta_l (\text{Re}[A_{||}^1 A_{\perp}^{1*}] + \hat{m}_l^2 \text{Re}[A_t^0 A_0^{0*} + A_t^1 A_0^{1*}]) \\ &\quad + \frac{3}{4} [1 - (1 - \hat{m}_l^2) \cos^2\theta_l] (|A_0^0|^2 + |A_0^1|^2) \\ &\quad + \frac{3}{8} [(1 + \hat{m}_l^2) + (1 - \hat{m}_l^2) \cos^2\theta_l] (|A_{||}^1|^2 + |A_{\perp}^1|^2). \end{aligned} \quad (4.28)$$

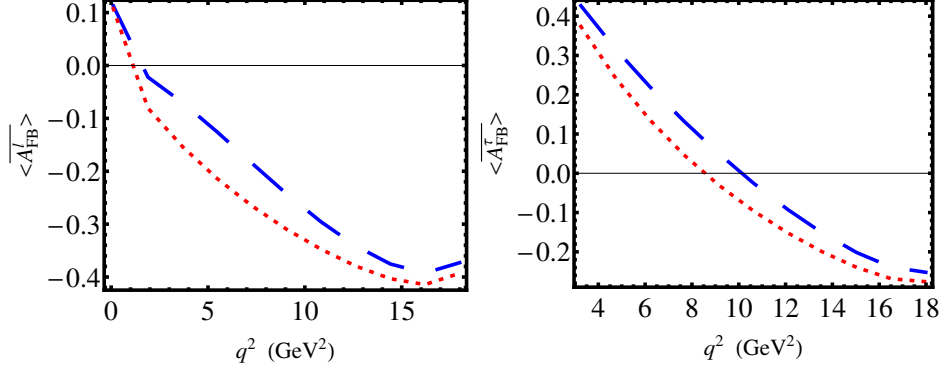


Figure 6. Same as Fig. 4 but for the asymmetry $\overline{\mathcal{A}_{FB}^l}$ in $B_s \rightarrow K\pi\ell\bar{\nu}_\ell$

The forward-backward asymmetry is defined as

$$\begin{aligned} A_{FB}^l &\equiv \left[\int_0^1 - \int_{-1}^0 \right] d\cos\theta_l \frac{d^3\Gamma}{dq^2 dm_{K\pi}^2 d\cos\theta_l} \\ &= \frac{3}{2} (\text{Re}[A_{\parallel}^1 A_{\perp}^{1*}] + \hat{m}_l^2 \text{Re}[A_t^0 A_0^{0*} + A_t^1 A_0^{1*}]), \end{aligned} \quad (4.29)$$

and the results for $\overline{\mathcal{A}_{FB}^l}$ are given in Fig. 6. The A_{\parallel}^1 and A_{\perp}^1 have different signs, and thus the $\overline{\mathcal{A}_{FB}^l}$ becomes negative when the \hat{m}_l^2 corrections become less important in the large q^2 region.

4.4 Distribution in the azimuthal angle ϕ

The angular distribution in ϕ is derived as

$$\frac{d^3\Gamma}{dq^2 dm_{K\pi}^2 d\phi} = a_\phi + b_\phi^c \cos\phi + b_\phi^s \sin\phi + c_\phi^c \cos(2\phi) + c_\phi^s \sin(2\phi), \quad (4.30)$$

with

$$\begin{aligned} a_\phi &= \frac{1}{2\pi} \frac{d^2\Gamma}{dq^2 dm_{K\pi}^2}, \\ b_\phi^c &= \frac{3}{16} \pi \int d\cos\theta_K I_5 = \frac{3\sqrt{3}}{32\sqrt{2}\pi} (\text{Re}[A_0^0 A_{\perp}^{1*}] - \hat{m}_l^2 \text{Re}[A_t^0 A_{\perp}^{1*}]), \\ b_\phi^s &= \frac{3}{16} \pi \int d\cos\theta_K I_7 = \frac{3\sqrt{3}}{32\sqrt{2}\pi} (\text{Im}[A_0^0 A_{\perp}^{1*}] - \hat{m}_l^2 \text{Im}[A_t^0 A_{\perp}^{1*}]), \\ c_\phi^c &= \frac{1}{2} \int d\cos\theta_K I_3 = \frac{1}{4\pi} \beta_l (|A_{\perp}^1|^2 - |A_{\parallel}^1|^2), \\ c_\phi^s &= \frac{1}{2} \int d\cos\theta_K I_9 = \frac{1}{2\pi} \beta_l \text{Im}[A_{\perp}^1 A_{\parallel}^{1*}]. \end{aligned} \quad (4.31)$$

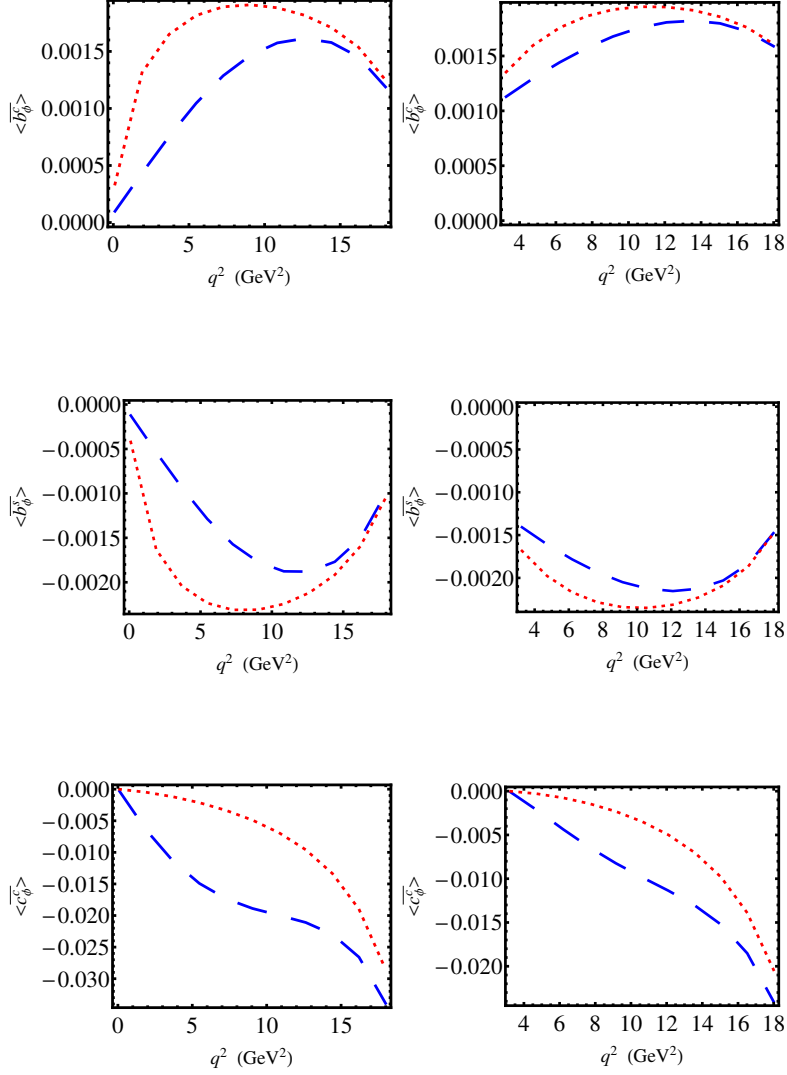


Figure 7. Same as Fig. 4 but for the normalised coefficients in the ϕ distributions of $\bar{B}_s \rightarrow K^0 \pi^+ \ell \bar{\nu}_\ell$

Since the complex phase in the P-wave amplitudes comes from the Breit-Wigner lineshape, the coefficient c_ϕ^s vanishes.

Numerical results for the normalised coefficients using the two sets of form factors are shown in Fig. 7, with the left panels for the light lepton and the right ones for the τ lepton, respectively. The coefficients b_ϕ^c and b_ϕ^s contain a very small prefactor, $3\sqrt{3}/(32\sqrt{2}\pi) \sim 0.037$, and thus are numerically tiny as shown in this figure. The c_ϕ^c is also small due to the cancellation between the $|A_\perp|^2$ and $|A_\parallel|^2$.

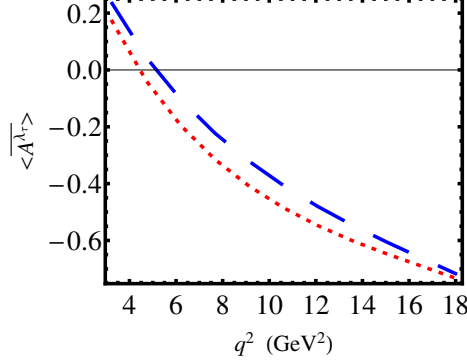


Figure 8. Same as Fig. 4 but for the polarisation distribution of $B_s \rightarrow K\pi\tau\bar{\nu}_\tau$

4.5 Polarisation of the τ lepton

We also give the polarised angular distributions as

$$\begin{aligned} \frac{d^5\Gamma(\lambda_\tau)}{dm_{K\pi}^2 dq^2 d\cos\theta_K d\cos\theta_l d\phi} = & \frac{3}{8} \left[I_1^{(\lambda_\tau)} + I_2^{(\lambda_\tau)} \cos(2\theta_l) + I_3^{(\lambda_\tau)} \sin^2\theta_l \cos(2\phi) \right. \\ & + I_4^{(\lambda_\tau)} \sin(2\theta_l) \cos\phi + I_5^{(\lambda_\tau)} \sin(\theta_l) \cos\phi + I_6^{(\lambda_\tau)} \cos\theta_l \\ & \left. + I_7^{(\lambda_\tau)} \sin(\theta_l) \sin\phi + I_8^{(\lambda_\tau)} \sin(2\theta_l) \sin\phi + I_9^{(\lambda_\tau)} \sin^2\theta_l \sin(2\phi) \right], \end{aligned} \quad (4.32)$$

with the coefficients

$$\begin{aligned} I_1^{(-1/2)} &= |A_0|^2 + \frac{3}{2}(|A_\perp|^2 + |A_\parallel|^2), \\ I_2^{(-1/2)} &= -|A_0|^2 + \frac{1}{2}(|A_\perp|^2 + |A_\parallel|^2), \\ I_3^{(-1/2)} &= |A_\perp|^2 - |A_\parallel|^2, \quad I_4^{(-1/2)} = 2[\text{Re}(A_0 A_\parallel^*)], \\ I_5^{(-1/2)} &= 4[\text{Re}(A_0 A_\perp^*)], \quad I_6^{(-1/2)} = 4[\text{Re}(A_\parallel A_\perp^*)], \\ I_7^{(-1/2)} &= 4[\text{Im}(A_0 A_\parallel^*)], \quad I_8^{(-1/2)} = 2[\text{Im}(A_0 A_\perp^*)], \\ I_9^{(-1/2)} &= 2[\text{Im}(A_\perp A_\parallel^*)]. \end{aligned} \quad (4.33)$$

The coefficients for $\lambda_\tau = 1/2$ are easily obtained by comparing Eq. (4.33) and Eq. (4.13).

The polarisation fraction for the τ -lepton is defined as

$$\begin{aligned} \overline{A^{\lambda_\tau}}(q^2, m_{K\pi}^2) &= \frac{d^2\Gamma^{(1/2)}/dq^2 dm_{K\pi}^2 - d^2\Gamma^{(-1/2)}/dq^2 dm_{K\pi}^2}{d^2\Gamma/dq^2 dm_{K\pi}^2} \\ &= \frac{(-1 + \hat{m}_l^2/2)(|A_0^0|^2 + |A_0^1|^2 + |A_\parallel^1|^2 + |A_\perp^1|^2) + \frac{3}{2}\hat{m}_l^2(|A_t^1|^2 + |A_t^0|^2)}{d^2\Gamma/dq^2 dm_{K\pi}^2} \end{aligned} \quad (4.34)$$

and we show the numerical results in Fig. 8.

4.6 $B^- \rightarrow \pi^+\pi^-\ell\bar{\nu}$

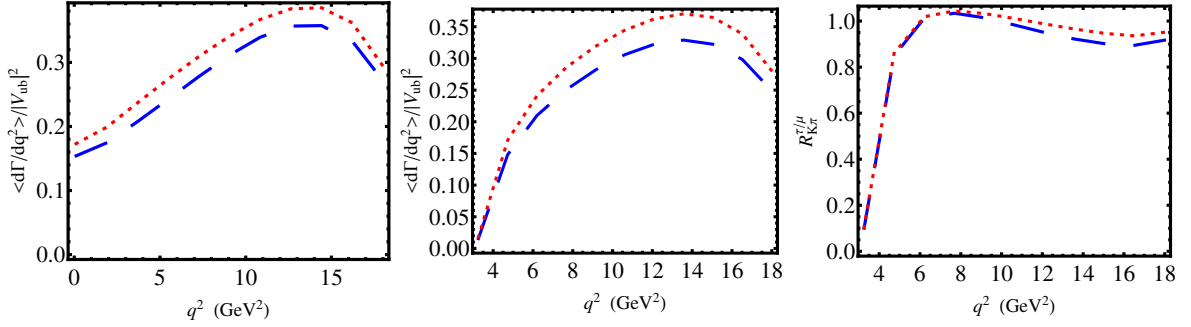


Figure 9. Similar as Fig. 4 but for the differential decay widths of the $B^- \rightarrow \pi^+\pi^-\ell\bar{\nu}$.

In this subsection, we shall update the predictions for the $B^- \rightarrow \pi^+\pi^-\ell\bar{\nu}$ process (for a recent calculation using dispersion relations matched to chiral perturbation theory, see [28]). For the $B \rightarrow \rho$ form factors, we take the results from the LCSR [7] and the LFQM [10] calculations.

We first stress the importance of considering the $\pi^+\pi^-$ spectrum distribution and the $\pi^+\pi^-$ final state interaction. To identify the ρ meson, the experimental measurements from the Babar collaboration on $B \rightarrow \rho l\bar{\nu}$ [4] have used the kinematical constraint

$$0.65 \text{ GeV} < m_{\pi\pi} < 0.85 \text{ GeV} . \quad (4.35)$$

In the narrow-width limit for the pure P-wave contributions, the integration of the lineshape should give

$$\int dm_{\pi\pi}^2 |L_\rho(m_{\pi\pi}^2)|^2 = 1 . \quad (4.36)$$

However, this integration in the selected kinematical region amounts to

$$\int_{0.65^2}^{0.85^2} dm_{\pi\pi}^2 |L_\rho(m_{\pi\pi}^2)|^2 = 0.59, \quad (4.37)$$

which is far below 1. A smaller value of $|V_{ub}|$ was found by the BaBar collaboration [4]:

$$|V_{ub}| = (2.75 \pm 0.24) \times 10^{-3}, \quad (4.38)$$

based on the data on $B \rightarrow \rho l\bar{\nu}$ in the range $0 < q^2 < 16 \text{ GeV}^2$ and theoretical results using the LCSR form factors. Here, theoretical errors from the $B \rightarrow \rho$ form factors are not taken into account in the experimental analysis [4]. This small value is also confirmed by a recent theoretical determination [75].

In our calculation, we suggest to choose $\delta_m = \Gamma_\rho$, corresponding to

$$\int_{(m_\rho - \Gamma_\rho)^2}^{(m_\rho + \Gamma_\rho)^2} dm_{\pi\pi}^2 |L_\rho(m_{\pi\pi}^2)|^2 = 0.70. \quad (4.39)$$

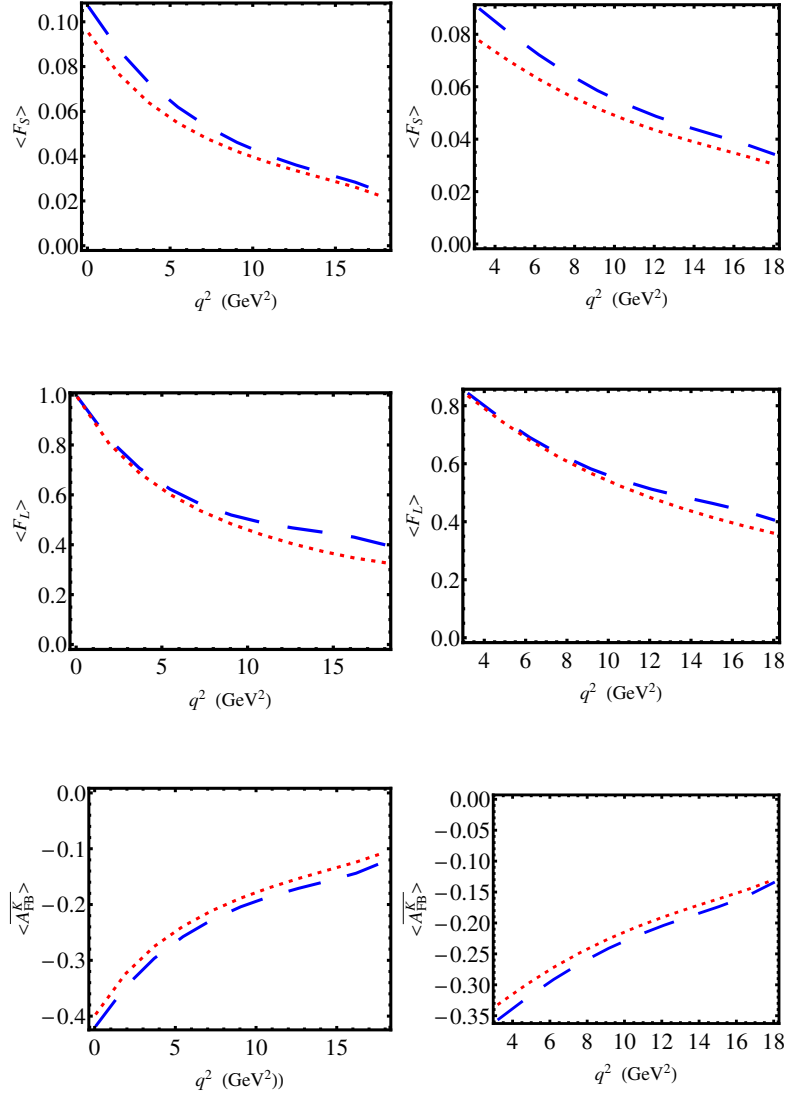


Figure 10. Similar as Fig. 5 but for the $B^- \rightarrow \pi^+ \pi^- \ell \bar{\nu}_\ell$.

This will increase the importance of $B \rightarrow \rho \ell \bar{\nu}$. On the other hand the S-wave lineshape in this region is also significant

$$\int_{(m_\rho - \Gamma_\rho)^2}^{(m_\rho + \Gamma_\rho)^2} dm_{\pi\pi}^2 |L_S(m_{\pi\pi}^2)|^2 = 0.09. \quad (4.40)$$

These effects should be taken into account in future experimental determinations.

Our results for integrated decay widths are collected in Tab. 6, and for the LFQM calculation, we have introduced 10% errors to the form factors, as indicated from Refs. [60–62]. The differential decay widths, polarisations, forward-backward asymmetries, and the τ -lepton polarisations are given in Figs. 9, 10, 11, 12, and 13, respectively. In these figures,

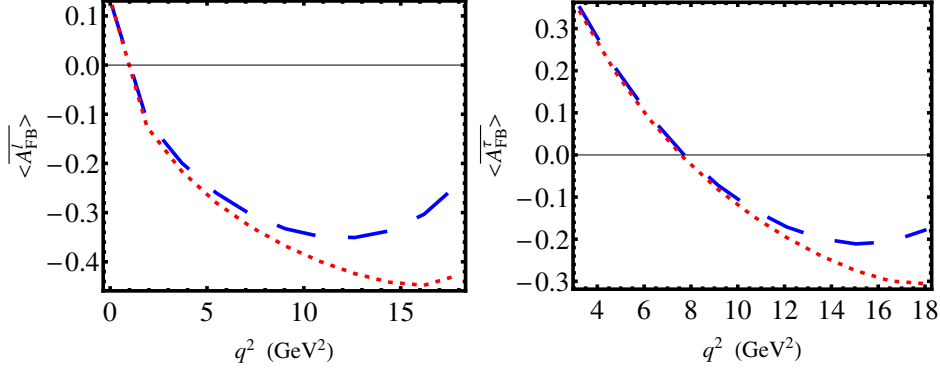


Figure 11. Similar as Fig. 6 but for the $B^- \rightarrow \pi^+ \pi^- \ell \bar{\nu}_\ell$

Table 6. Integrated decay widths for $B^- \rightarrow \pi^+ \pi^- \ell \bar{\nu}$: $\Delta\zeta_{\pi\pi}^\ell(q_l^2, q_u^2)$. Results are given in units of ps^{-1} . The S-wave contributions are obtained with form factors calculated in the PQCD approach.

		S-Wave	P-Wave	Total	$f_S(\%)$
$\Delta\zeta_{\pi\pi}^\mu(0, 4)$	LFQM	0.068 ± 0.038	0.656 ± 0.137	0.723 ± 0.176	9.41
	LCSR	0.068 ± 0.038	0.754 ± 0.128	0.822 ± 0.166	8.27
$\Delta\zeta_{\pi\pi}^\mu(4, 8)$	LFQM	0.068 ± 0.038	0.984 ± 0.206	1.05 ± 0.247	6.48
	LCSR	0.068 ± 0.038	1.11 ± 0.205	1.18 ± 0.241	5.76
$\Delta\zeta_{\pi\pi}^\mu(8, 12)$	LFQM	0.064 ± 0.036	1.29 ± 0.268	1.35 ± 0.308	4.74
	LCSR	0.064 ± 0.036	1.41 ± 0.261	1.47 ± 0.301	4.35
$\Delta\zeta_{\pi\pi}^\mu(12, 16)$	LFQM	0.054 ± 0.03	1.42 ± 0.294	1.47 ± 0.329	3.67
	LCSR	0.054 ± 0.03	1.53 ± 0.297	1.58 ± 0.331	3.42
$\Delta\zeta_{\pi\pi}^\mu(0, 16)$	LFQM	0.254 ± 0.143	4.34 ± 0.916	4.6 ± 1.05	5.52
	LCSR	0.254 ± 0.143	4.8 ± 0.895	5.06 ± 1.03	5.02
$\Delta\zeta_{\pi\pi}^\tau(m_\tau^2, 8)$	LFQM	0.069 ± 0.039	0.793 ± 0.166	0.862 ± 0.205	8.
	LCSR	0.069 ± 0.039	0.92 ± 0.171	0.988 ± 0.211	6.98
$\Delta\zeta_{\pi\pi}^\tau(8, 12)$	LFQM	0.074 ± 0.042	1.15 ± 0.241	1.22 ± 0.288	6.07
	LCSR	0.074 ± 0.042	1.31 ± 0.246	1.38 ± 0.293	5.36
$\Delta\zeta_{\pi\pi}^\tau(12, 16)$	LFQM	0.14 ± 0.079	2.43 ± 0.511	2.57 ± 0.59	5.45
	LCSR	0.14 ± 0.079	2.76 ± 0.531	2.9 ± 0.61	4.83
$\Delta\zeta_{\pi\pi}^\tau(m_\tau^2, 16)$	LFQM	0.209 ± 0.117	3.22 ± 0.681	3.43 ± 0.797	6.09
	LCSR	0.209 ± 0.117	3.68 ± 0.702	3.89 ± 0.818	5.37

the dashed and dotted lines correspond to the LFQM and LCSR form factors. The S-wave fraction ranges from approximately 4% to 10% depending on the q^2 .

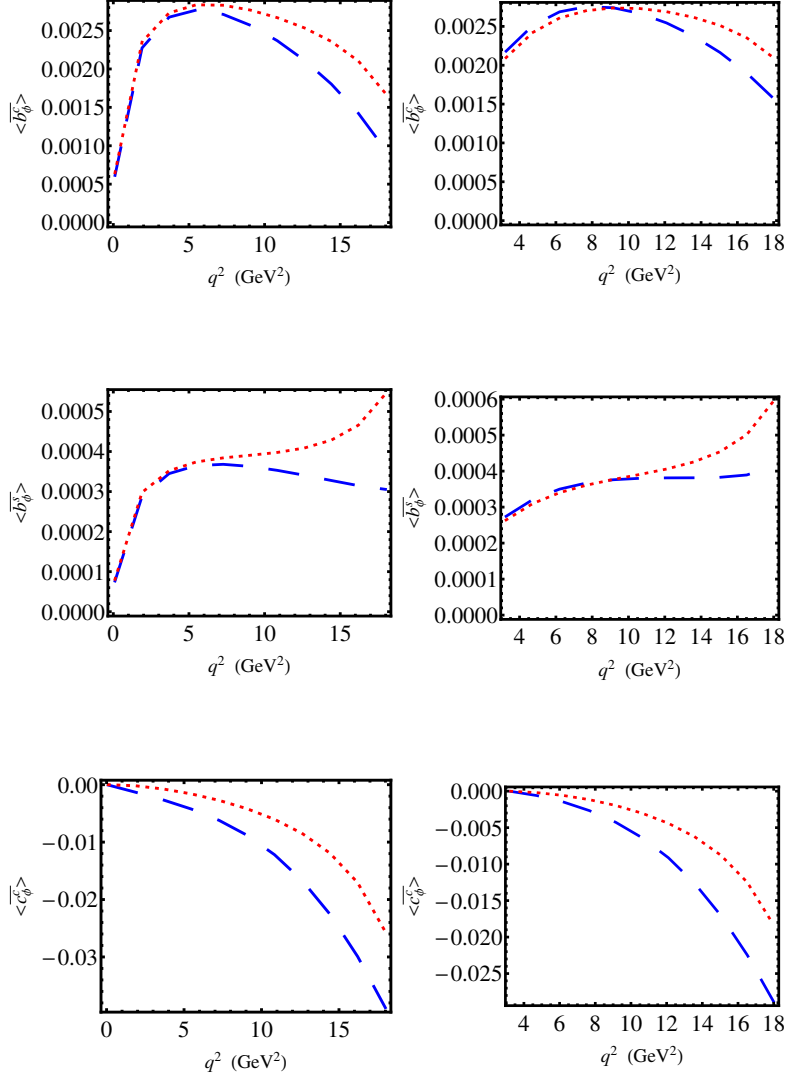


Figure 12. Similar as Fig. 7 but for the $B^- \rightarrow \pi^+ \pi^- \ell \bar{\nu}_\ell$

4.7 $B^- \rightarrow K^+ K^- \ell \bar{\nu}$

For the first time, we provide predictions for the $B^- \rightarrow K^+ K^- \ell \bar{\nu}$ decay rates. Apparently, the P-wave resonance contribution is highly suppressed, as no resonance can be copiously produced in the $b \rightarrow u$ transition and has a large decay branching ratio into $K^+ K^-$. The contribution from ϕ - ω mixing, whose effects in B decays have been stressed in Ref. [76–78], is given by

$$\mathcal{B}(B^- \rightarrow (K^+ K^-)_P \ell \bar{\nu}) \simeq \frac{1}{2} \mathcal{B}(B^- \rightarrow \phi \ell \bar{\nu}) = \sin^2 \theta \mathcal{B}(B^- \rightarrow \omega \ell \bar{\nu}) \sim 0.4 \times 10^{-6}. \quad (4.41)$$

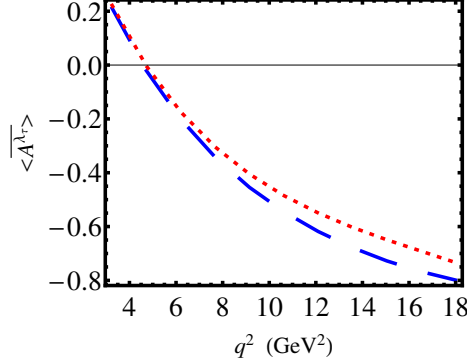


Figure 13. Similar as Fig. 8 but for the $B^- \rightarrow \pi^+ \pi^- \ell \bar{\nu}_\ell$

where the $\mathcal{B}(B^- \rightarrow \omega \ell \bar{\nu}) = (1.19 \pm 0.32 \pm 0.05) \times 10^{-4}$ is taken from Ref. [79] and the $\omega - \phi$ mixing angle $\theta = (3.4 \pm 0.3)^\circ$ is extracted from the ω and ϕ decays in Ref. [80].

It is also necessary to consider the D wave contributions from the $f_2(1270)$

$$\mathcal{B}(B^- \rightarrow (K^+ K^-)_D \ell \bar{\nu}) = 4.6\% \times 0.52 \times 10^{-4} = 2.3 \times 10^{-6}, \quad (4.42)$$

where we have used the estimate of the $\mathcal{B}(B \rightarrow f_2 \ell \bar{\nu})$ from Ref. [51].

The S-wave $K^+ K^-$ can have isospin 0 and isospin 1, and here we focus on the isospin 0 contribution. The $f_0(980)$ contribution is suppressed due to phase space. Integrating from the threshold to the $f_2(1270)$ mass, we have

$$\int_{4m_K^2}^{m_{f_2(1270)}^2} dm_{K\bar{K}}^2 |L_S(m_{K\bar{K}}^2)| = 0.8\%, \quad (4.43)$$

and thus

$$\mathcal{B}(B^- \rightarrow (K^+ K^-)_S \ell \bar{\nu}) = 0.8\% \times 1.8 \times 10^{-4} = 1.4 \times 10^{-6}, \quad (4.44)$$

where the transition induced by $b \rightarrow u \ell \bar{\nu}$ is calculated using the $B \rightarrow a_0(980)$ form factors. The measurements of this channel at the LHCb facility and the Super B factory in the future may directly test our mechanism and constrain the parameters in this approach.

5 Conclusions

In this work, we have analysed the $\bar{B}_s^0 \rightarrow K^+ \ell^- \bar{\nu}$ and $\bar{B}_s^0 \rightarrow K^{*+} \ell^- \bar{\nu}$ decays in the pursuit of the extraction of the CKM matrix element $|V_{ub}|$. We have calculated differential and integrated decay widths in units of $|V_{ub}|^2$ based on three sets of $B_s \rightarrow K$ form factors. Although parametric errors in the decay widths will drop out in ratios, the three sets of results have different behaviours especially in the large q^2 region. Such discrepancies will be removed once Lattice QCD is able to predict the form factors at large q^2 .

For the decay $B_s \rightarrow K\pi l\bar{\nu}$, we have derived the angular distributions with the inclusion of the S-wave $K\pi$ contributions, from which a number of angular observables including partial widths, polarisation, or the forward-backward asymmetry, can be defined. Using the recent Lattice QCD and the light-cone sum rule results for the $B_s \rightarrow K^*$ form factors, we have discussed the possible S-wave effects on angular distributions. We found that the S-wave contribution to partial widths can reach 10% to 20% depending on the momentum transfer, and thus their impact can not be ignored. We have also updated the results on $B \rightarrow \pi^+\pi^-\ell\bar{\nu}$ and discussed the S-wave $\pi\pi$ contributions. Measurements of these channels in the future can not only be used to extract $|V_{ub}|$ but also provide useful information to access the $K\pi/\pi\pi$ strong phase.

Acknowledgements

We thank Michael Döring for collaboration in the early stage of this work, and Vladimir Galkin and Bastian Kubis for useful discussions. This work is supported in part by the DFG and the NSFC through funds provided to the Sino-German CRC 110 “Symmetries and the Emergence of Structure in QCD”, and the EU “I3HP Study of Strongly Interacting Matter” under the Seventh Framework Program.

A Angular coefficients

Substituting the expressions A_i into the angular coefficients, we obtain the general expressions

$$\begin{aligned}
I_1 &= \sum_{J=0,\dots} \left\{ |Y_J^0(\theta_K, 0)|^2 [(1 + \hat{m}_l^2) |A_0^J|^2 + 2\hat{m}_l^2 |A_t^J|^2] \right. \\
&\quad + 2 \sum_{J'=J+1,\dots} Y_J^0(\theta_K, 0) Y_{J'}^0(\theta_K, 0) \left[\cos(\delta_0^J - \delta_0^{J'}) |A_0^J| |A_0^{J'*}| + 2\hat{m}_l^2 \cos(\delta_t^J - \delta_t^{J'}) |A_t^J| |A_t^{J'*}| \right] \\
&\quad + \frac{3 + \hat{m}_l^2}{2} \sum_{J=1,\dots} \left\{ |Y_J^{-1}(\theta_K, 0)|^2 [|A_\perp^J|^2 + |A_\parallel^J|^2] \right. \\
&\quad + \sum_{J'=J+1,\dots} Y_J^{-1}(\theta_K, 0) Y_{J'}^{-1}(\theta_K, 0) \left[2 \cos(\delta_\perp^J - \delta_\perp^{J'}) |A_\perp^J| |A_\perp^{J'*}| \right] \Big\}, \\
I_2 &= -\beta_l \sum_{J=0,\dots} \left\{ |Y_J^0|^2 |A_0^J(\theta_K, 0)|^2 + 2 \sum_{J'=J+1,\dots} Y_J^0(\theta_K, 0) Y_{J'}^0(\theta_K, 0) \cos(\delta_0^J - \delta_0^{J'}) |A_0^J A_0^{J'}| \right\} \\
&\quad + \frac{1}{2} \beta_l \sum_{J=1,\dots} \left\{ |Y_J^{-1}(\theta_K, 0)|^2 (|A_\perp^J|^2 + |A_\parallel^J|^2) \right. \\
&\quad + 2 \sum_{J'=J+1} Y_J^{-1}(\theta_K, 0) Y_{J'}^{-1}(\theta_K, 0) \left[\cos(\delta_\perp^J - \delta_\perp^{J'}) |A_\perp^J A_\perp^{J'}| + \cos(\delta_\parallel^J - \delta_\parallel^{J'}) |A_\parallel^J A_\parallel^{J'}| \right] \Big\}, \\
I_3 &= \beta_l \sum_{J=1,\dots} \left\{ |Y_J^{-1}(\theta_K, 0)|^2 (|A_\perp^J|^2 - |A_\parallel^J|^2) \right. \\
&\quad + 2 \sum_{J'=J+1} Y_J^{-1}(\theta_K, 0) Y_{J'}^{-1}(\theta_K, 0) \left[\cos(\delta_\perp^J - \delta_\perp^{J'}) |A_\perp^J A_\perp^{J'}| - \cos(\delta_\parallel^J - \delta_\parallel^{J'}) |A_\parallel^J A_\parallel^{J'}| \right] \Big\}, \\
I_4 &= 2\beta_l \sum_{J=0,\dots} \sum_{J'=1,\dots} \left[Y_J^0(\theta_K, 0) Y_{J'}^{-1}(\theta_K, 0) |A_0^J A_\parallel^{J'*}| \cos(\delta_0^J - \delta_\parallel^{J'}) \right], \\
I_5 &= 4 \sum_{J=0,\dots} \sum_{J'=1,\dots} Y_J^0(\theta_K, 0) Y_{J'}^{-1}(\theta_K, 0) \left[|A_0^J A_\perp^{J'*}| \cos(\delta_0^J - \delta_\perp^{J'}) - \hat{m}_l^2 |A_t^J A_\parallel^{J'*}| \cos(\delta_t^J - \delta_\parallel^{J'}) \right], \\
I_6 &= 4 \sum_{J,J'=1,\dots} \left\{ Y_J^{-1}(\theta_K, 0) Y_{J'}^{-1}(\theta_K, 0) |A_\parallel^J A_\perp^{J'*}| \cos(\delta_\parallel^J - \delta_\perp^{J'}) \right\} \\
&\quad + \hat{m}_l^2 \sum_{J,J'=0,\dots} \left\{ Y_J^0(\theta_K, 0) Y_{J'}^0(\theta_K, 0) |A_t^J A_0^{J'*}| \cos(\delta_t^J - \delta_0^{J'}) \right\}, \\
I_7 &= 4 \sum_{J=0,\dots} \sum_{J'=1,\dots} Y_J^0(\theta_K, 0) Y_{J'}^{-1}(\theta_K, 0) \left[|A_0^J A_\parallel^{J'*}| \sin(\delta_0^J - \delta_\parallel^{J'}) - \hat{m}_l^2 |A_t^J A_\perp^{J'*}| \sin(\delta_t^J - \delta_\perp^{J'}) \right], \\
I_8 &= 2\beta_l \sum_{J=0,\dots} \sum_{J'=1,\dots} \left[Y_J^0(\theta_K, 0) Y_{J'}^{-1}(\theta_K, 0) |A_0^J A_\perp^{J'*}| \sin(\delta_0^J - \delta_\perp^{J'}) \right], \\
I_9 &= 2\beta_l \sum_{J=1,\dots} \sum_{J'=1,\dots} \left[Y_J^{-1}(\theta_K, 0) Y_{J'}^{-1}(\theta_K, 0) |A_\perp^J A_\parallel^{J'*}| \sin(\delta_\perp^J - \delta_\parallel^{J'}) \right]. \tag{A.1}
\end{aligned}$$

References

- [1] Y. Amhis *et al.* [Heavy Flavor Averaging Group Collaboration], arXiv:1207.1158 [hep-ex].
- [2] J. Beringer *et al.* [Particle Data Group Collaboration], Phys. Rev. D **86**, 010001 (2012).
- [3] A. Khodjamirian, T. Mannel, N. Offen and Y.-M. Wang, Phys. Rev. D **83**, 094031 (2011) [arXiv:1103.2655 [hep-ph]].
- [4] P. del Amo Sanchez *et al.* [BaBar Collaboration], Phys. Rev. D **83**, 032007 (2011) [arXiv:1005.3288 [hep-ex]].
- [5] A. Bharucha, JHEP **1205**, 092 (2012) [arXiv:1203.1359 [hep-ph]].
- [6] R. R. Horgan, Z. Liu, S. Meinel and M. Wingate, arXiv:1310.3722 [hep-lat].
- [7] P. Ball and R. Zwicky, Phys. Rev. D **71**, 014029 (2005) [hep-ph/0412079].
- [8] W.-F. Wang and Z.-J. Xiao, Phys. Rev. D **86**, 114025 (2012) [arXiv:1207.0265 [hep-ph]].
- [9] R. N. Faustov and V. O. Galkin, Phys. Rev. D **87**, 094028 (2013) [arXiv:1304.3255].
- [10] H.-Y. Cheng, C.-K. Chua and C.-W. Hwang, Phys. Rev. D **69**, 074025 (2004) [hep-ph/0310359].
- [11] C.-D. Lu, W. Wang and Z.-T. Wei, Phys. Rev. D **76**, 014013 (2007) [hep-ph/0701265 [HEP-PH]].
- [12] R. C. Verma, J. Phys. G **39**, 025005 (2012) [arXiv:1103.2973 [hep-ph]].
- [13] F. Kruger, L. M. Sehgal, N. Sinha and R. Sinha, Phys. Rev. D **61**, 114028 (2000) [Erratum-ibid. D **63**, 019901 (2001)] [hep-ph/9907386].
- [14] C.-D. Lu and W. Wang, Phys. Rev. D **85**, 034014 (2012) [arXiv:1111.1513 [hep-ph]].
- [15] M. Döring, U.-G. Meißner and W. Wang, JHEP **1310**, 011 (2013) [arXiv:1307.0947 [hep-ph]].
- [16] R.-H. Li, C.-D. Lu and W. Wang, Phys. Rev. D **83**, 034034 (2011) [arXiv:1012.2129 [hep-ph]].
- [17] D. Becirevic and A. Tayduganov, Nucl. Phys. B **868**, 368 (2013) [arXiv:1207.4004 [hep-ph]].
- [18] J. Matias, Phys. Rev. D **86**, 094024 (2012) [arXiv:1209.1525 [hep-ph]].
- [19] T. Blake, U. Egede and A. Shires, JHEP **1303**, 027 (2013) [arXiv:1210.5279 [hep-ph]].
- [20] C. Bobeth, G. Hiller and D. van Dyk, Phys. Rev. D **87**, 034016 (2013) [arXiv:1212.2321 [hep-ph]].
- [21] S. Descotes-Genon, T. Hurth, J. Matias and J. Virto, JHEP **1305**, 137 (2013) [arXiv:1303.5794 [hep-ph]].
- [22] S. Descotes-Genon, J. Matias and J. Virto, Phys. Rev. D **88**, 074002 (2013) [arXiv:1307.5683 [hep-ph]].
- [23] F. A. Berends, A. Donnachie and G. C. Oades, Phys. Rev. **171**, 1457 (1968).
- [24] G. Kopp, G. Kramer, G. A. Schuler and W. F. Palmer, Z. Phys. C **48**, 327 (1990).
- [25] C. L. Y. Lee, M. Lu and M. B. Wise, Phys. Rev. D **46**, 5040 (1992).
- [26] B. Ananthanarayan and K. Shivaraj, Phys. Lett. B **628**, 223 (2005) [hep-ph/0508116].
- [27] S. Faller, T. Feldmann, A. Khodjamirian, T. Mannel and D. van Dyk, arXiv:1310.6660 [hep-ph].

- [28] C. Hanhart, X.-W. Kang, B. Kubis and U.-G. Meißner, arXiv:1312.1193 [hep-ph].
- [29] P. Buettiker, S. Descotes-Genon and B. Moussallam, Eur. Phys. J. C **33**, 409 (2004) [hep-ph/0310283].
- [30] S. Descotes-Genon and B. Moussallam, Eur. Phys. J. C **48**, 553 (2006) [hep-ph/0607133].
- [31] S. Gardner and U.-G. Meißner, Phys. Rev. D **65**, 094004 (2002) [hep-ph/0112281].
- [32] J. Gasser and U.-G. Meißner, Nucl. Phys. B **357**, 90 (1991).
- [33] J. A. Oller, E. Oset and J. E. Palomar, Phys. Rev. D **63**, 114009 (2001) [hep-ph/0011096].
- [34] U.-G. Meißner and J. A. Oller, Nucl. Phys. A **679**, 671 (2001) [hep-ph/0005253].
- [35] M. Frink, B. Kubis and U.-G. Meißner, Eur. Phys. J. C **25**, 259 (2002) [hep-ph/0203193].
- [36] J. Bijnens and P. Talavera, Nucl. Phys. B **669**, 341 (2003) [hep-ph/0303103].
- [37] T. A. Lähde and U.-G. Meißner, Phys. Rev. D **74**, 034021 (2006) [hep-ph/0606133].
- [38] Z.-H. Guo, J. A. Oller and J. Ruiz de Elvira, Phys. Rev. D **86**, 054006 (2012) [arXiv:1206.4163 [hep-ph]].
- [39] J. F. Donoghue, J. Gasser and H. Leutwyler, Nucl. Phys. B **343**, 341 (1990).
- [40] M. Jamin, J. A. Oller and A. Pich, Nucl. Phys. B **587**, 331 (2000) [hep-ph/0006045].
- [41] M. Jamin, J. A. Oller and A. Pich, Nucl. Phys. B **622**, 279 (2002) [hep-ph/0110193].
- [42] M. Jamin, J. A. Oller and A. Pich, Phys. Rev. D **74**, 074009 (2006) [hep-ph/0605095].
- [43] V. Bernard and E. Passemar, Phys. Lett. B **661**, 95 (2008) [arXiv:0711.3450 [hep-ph]].
- [44] V. Bernard and E. Passemar, JHEP **1004**, 001 (2010) [arXiv:0912.3792 [hep-ph]].
- [45] J. P. Lees *et al.* [BaBar Collaboration], Phys. Rev. D **88**, 031102 (2013) [arXiv:1207.0698 [hep-ex]].
- [46] I. Adachi *et al.* [Belle Collaboration], Phys. Rev. Lett. **110**, 131801 (2013) [arXiv:1208.4678 [hep-ex]].
- [47] T. Hurth and F. Mahmoudi, Rev. Mod. Phys. **85**, 795 (2013) [arXiv:1211.6453 [hep-ph]].
- [48] J. P. Lees *et al.* [BaBar Collaboration], Phys. Rev. Lett. **109**, 101802 (2012) [arXiv:1205.5442 [hep-ex]].
- [49] A. Sibidanov *et al.* [Belle Collaboration], Phys. Rev. D **88**, 032005 (2013) [arXiv:1306.2781 [hep-ex]].
- [50] H. Hatanaka and K.-C. Yang, Eur. Phys. J. C **67**, 149 (2010) [arXiv:0907.1496 [hep-ph]].
- [51] W. Wang, Phys. Rev. D **83**, 014008 (2011) [arXiv:1008.5326 [hep-ph]].
- [52] K.-C. Yang, Phys. Lett. B **695**, 444 (2011) [arXiv:1010.2944 [hep-ph]].
- [53] C. M. Bouchard, G. P. Lepage, C. J. Monahan, H. Na and J. Shigemitsu, arXiv:1310.3207 [hep-lat].
- [54] G. Duplancic and B. Melic, Phys. Rev. D **78**, 054015 (2008) [arXiv:0805.4170 [hep-ph]].
- [55] Y.-Y. Keum, H.-N. Li and A. I. Sanda, Phys. Lett. B **504**, 6 (2001) [hep-ph/0004004].
- [56] Y. Y. Keum, H.-N. Li and A. I. Sanda, Phys. Rev. D **63**, 054008 (2001) [hep-ph/0004173].
- [57] C.-D. Lu, K. Ukai and M.-Z. Yang, Phys. Rev. D **63**, 074009 (2001) [hep-ph/0004213].

- [58] C.-D. Lu and M.-Z. Yang, Eur. Phys. J. C **23**, 275 (2002) [hep-ph/0011238].
- [59] H.-N. Li, Y.-L. Shen and Y.-M. Wang, Phys. Rev. D **85**, 074004 (2012) [arXiv:1201.5066 [hep-ph]].
- [60] C.-H. Chen, Y.-L. Shen and W. Wang, Phys. Lett. B **686**, 118 (2010) [arXiv:0911.2875 [hep-ph]].
- [61] W. Wang, Y.-L. Shen and C.-D. Lu, Phys. Rev. D **79**, 054012 (2009) [arXiv:0811.3748 [hep-ph]].
- [62] X.-X. Wang, W. Wang and C.-D. Lu, Phys. Rev. D **79**, 114018 (2009) [arXiv:0901.1934 [hep-ph]].
- [63] C.-H. Chen and H.-N. Li, Phys. Lett. B **561**, 258 (2003) [hep-ph/0209043].
- [64] H.-Y. Cheng and C.-K. Chua, arXiv:1308.5139 [hep-ph].
- [65] Z.-H. Zhang, X.-H. Guo and Y.-D. Yang, Phys. Rev. D **87**, 076007 (2013) [arXiv:1303.3676 [hep-ph]].
- [66] U. -G. Meißner and W. Wang, arXiv:1312.3087 [hep-ph].
- [67] M. Diehl, Phys. Rept. **388**, 41 (2003) [hep-ph/0307382].
- [68] H.-Y. Cheng, C.-K. Chua and K.-C. Yang, Phys. Rev. D **73**, 014017 (2006) [hep-ph/0508104].
- [69] R.-H. Li, C.-D. Lu, W. Wang and X.-X. Wang, Phys. Rev. D **79**, 014013 (2009) [arXiv:0811.2648 [hep-ph]].
- [70] J. Bijnens and I. Jemos, Nucl. Phys. B **840**, 54 (2010) [Erratum-ibid. B **844**, 182 (2011)] [arXiv:1006.1197 [hep-ph]].
- [71] J. Bijnens and I. Jemos, Nucl. Phys. B **846**, 145 (2011) [arXiv:1011.6531 [hep-ph]].
- [72] J. A. Oller and E. Oset, Nucl. Phys. A **620**, 438 (1997) [Erratum-ibid. A **652**, 407 (1999)] [hep-ph/9702314].
- [73] P. del Amo Sanchez *et al.* [BaBar Collaboration], Phys. Rev. D **83**, 072001 (2011) [arXiv:1012.1810 [hep-ex]].
- [74] R. Aaij *et al.* [LHCb Collaboration], JHEP **1308**, 131 (2013) [arXiv:1304.6325 [hep-ex]].
- [75] J. M. Flynn, Y. Nakagawa, J. Nieves and H. Toki, Phys. Lett. B **675**, 326 (2009) [arXiv:0812.2795 [hep-ph]].
- [76] M. Gronau and J. L. Rosner, Phys. Lett. B **666**, 185 (2008) [arXiv:0806.3584 [hep-ph]].
- [77] Y. Li, C.-D. Lu and W. Wang, Phys. Rev. D **80**, 014024 (2009) [arXiv:0901.0648 [hep-ph]].
- [78] Z.-Q. Zhang, H.-F. Ou and L.-X. Lu, J. Phys. G **38**, 095005 (2011).
- [79] I. Adachi *et al.* [Belle Collaboration], arXiv:0812.1414 [hep-ex].
- [80] A. Kucukarslan and U.-G. Meißner, Mod. Phys. Lett. A **21**, 1423 (2006) [hep-ph/0603061].